

BACHELOR THESIS

Volume estimation of Styggedalsbreen glacier

Application of Ground Penetrating Radar for ice thickness measurement, mapping of subglacial bed topography, and volume estimation of Styggedalsbreen glacier.

by

102, Sandnes, Gaute Haugen

108, Bryn, Christian Rekve

124, Bakken, Skjalg Lie

Geology and Geohazards

GE 491

10.06.2014



Agreement regarding the electronical deposit of scientific publications in HiSF Brage – Institutional archive of Sogn og Fjordane University College

The author(s) hereby give(s) Sogn og Fjordane University College the right to make this thesis available in HiSF Brage provided that the thesis is awarded *grade B* or better.

I guarantee that I - together with possible co-authors - have the right of authorship to the material thus have legal rights to allow HiSF to publish the material in Brage.

I guarantee that I have no knowledge or suspicion indicating that this material is illegal according to Norwegian law.

Please fill in your candidate number and name below and tick off the appropriate answer:

102, Sandnes, Gaute Haugen

YES NO

108, Bryn, Christian Rekve

YES NO

124, Bakken, Skjalg Lie

YES NO

Abstract

If all glaciers in Norway melt away, the sea level would rise ~ 0.34 mm (Nesje et al. 2008).

Small valley glaciers respond fast to climate changes, but are also highly affected by short-term fluctuations in local precipitation and temperature. The purpose of this bachelor thesis is to use Ground Penetrating Radar (GPR) to estimate the volume of Styggedalsbreen through mapping of the bottom topography and modelling of the glacier thickness. Styggedalsbreen has a surface area of ~ 1.85 km² and is located in a part of Jotunheimen called Hurrungane. A total of 3 field excursions were carried out in the period August 2013-March 2014; two in August/September and one in March. A GPR system from Malå geoscience was used to survey more than 60 profiles in total, both north-south and east-west. Because of a combination of equipment failure and poor data quality, of these 60 profiles, only 11 were used in the final model to calculate a volume estimate. Ten of these profiles were made in March 2014 using a 50 MHz rough terrain antenna (RTA), while one was made in September 2013 with a 100 MHz RTA. After the data collection was complete, processing software like RadExplorer and Reflex2D-Quick (R2DQ) was used to process and interpret the profiles and determine the glacier thickness. Geographic information system (GIS) software was used to plot the profiles, interpolate data for areas where no measurements were done, and calculate the volume estimate. The final ice thickness model (figure) presents an estimated volume of 0.053 km³ ± 15 %, a maximum depth of 98.7 ± 8 m, a mean ice depth of 26.8 ± 8 m, and a subglacial U-shaped bed topography typical for glacier eroded alleys.

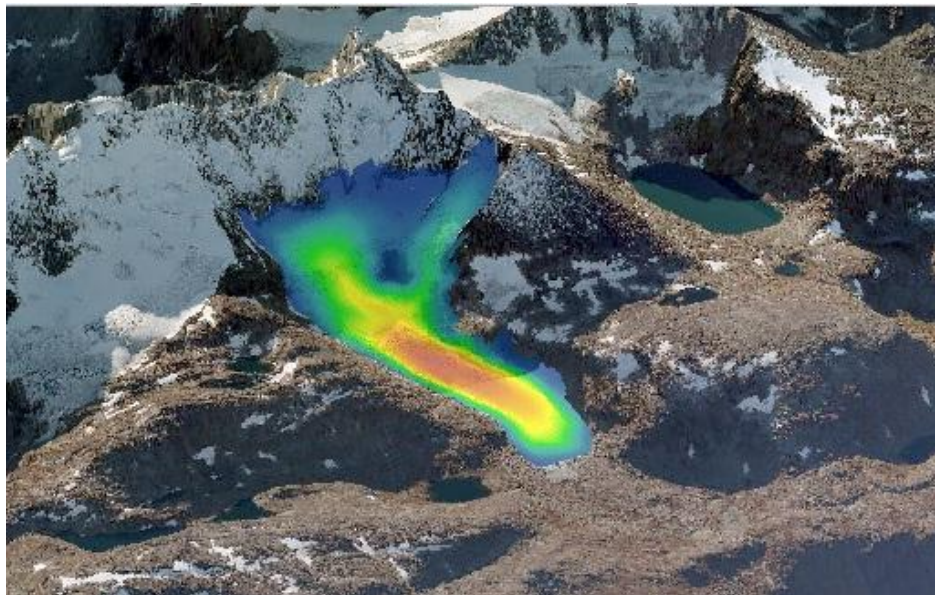


Figure: Ice thickness model of Styggedalsbreen seen from the North-east. Red areas mark the greatest ice thickness. Aerial photo: Bygdin 2008 (Norge I bilder).

Table of contents

1	Introduction	1
2	Study Area	4
2.1	Location.....	4
2.2	Glacial features	5
2.3	Climate	8
2.4	Geology	9
3	Methodology.....	12
3.1	Introduction	12
3.2	Principle of ground penetrating radar	13
3.3	Properties of materials	14
3.3.1	Electric Conductivity	14
3.3.2	Relative Permittivity.....	15
3.3.3	Velocity and depth calculation.....	16
3.4	EM wave propagation	17
3.4.1	Attenuation	18
3.4.2	Hyperbolas	20
3.4.3	Side-swipes.....	21
3.5	GPR settings	22
3.6	Processing of GPR profiles	23
3.7	GPS data.....	27
4	Results.....	30
4.1	Data collection	30
4.2	Interpretation.....	33
4.3	Ice thickness interpolation.....	36
4.3.1	2D-interpolation.....	36
4.3.2	3D-interpolation.....	37
4.4	Subglacial topography and variations in ice thickness	40
4.5	Volume estimate.....	43
4.5.1	LIA volume estimate	45
4.5.2	Volume-area empirical estimate.....	45

5	Discussion.....	46
5.1	Data collection	46
5.2	Interpretation and interpolation	47
5.3	Volume estimations	49
6	Conclusion.....	51
	Acknowledgements.....	52
	References	53
	Appendix A:.....	57
	Processing tools (with values):.....	57
	List of abbreviations:.....	58
	Appendix B:	59
	Appendix attached to CD-R.....	59

1 Introduction

Global mean sea level (GMSL) is currently rising by 3.2 mm/yr (1993-2010) in response to melting glaciers and ice caps in Antarctica and Greenland, as well as thermal expansion of sea water (Church et al. 2014). Depending on future climate developments, models predict a further rise of between 0.52 m and 0.98 m by 2100 (Church et al. 2014) in response to global warming. IPCC (International Panel of Climate Change) has estimated that the global mean temperature during the 21st century will rise between 1.1°C and 2.9°C as a best case scenario, and 2.4 to 6.4 °C as a worst case scenario (Stocker et al. 2014). This is a global mean change, and the values are not uniform around the globe.

The ice sheets of Antarctica and Greenland have the potential to increase sea level by 65 m if they were to melt (IPCC, 2001). However, a catastrophic event like that is not something that is likely to happen in the near future, with a current annual mean temperature in Antarctica of -48.3°C (Weatherbase, 2014). The sea level changes observed today are primarily the result of thermal expansion of sea water, and melting of glaciers located outside of Antarctica and Greenland. In the period 1993-2010, thermal expansion of sea water contributed 1.1 mm/yr, melting glaciers 0.76 mm/yr and glaciers on Greenland and Antarctica, 0.33 mm/yr and 0.27 mm/yr respectively (Table 1). This partly reflects the fact that smaller glaciers react faster to climate change (Salinger, J. et al. 2008) and will therefore be gone long before the ice sheets in Greenland and Antarctica. This highlights the importance of volume and mass balance studies of glaciers, since knowing the amount of water stored in glaciers will help predict sea level rise in the future. However, often no measurements of glacier volume exist, and empirical volume-area methods are applied to find an estimated volume of glaciers and ice caps from satellite and aerial photos (Yde et al. 2014). These methods have been developed using volume data from radio echo sounding of 144 glaciers in Europe, North-America, central-Asia and the Arctic (Bahr et al.2009). Overall, this is the most up to date method to find the volume of earth's glaciers and ice caps, but it may lead to significant uncertainties in volume estimates since it assumes that the glaciers and ice caps are in a state of equilibrium. The fact is that almost all glaciers and ice caps are in disequilibrium with their local climate (Yde et al. 2014), and are either increasing or decreasing in size due to the varying response time of glaciers and ice caps (Salinger, J. et al. 2008). New volume estimates from individual glaciers will be of crucial aid in the process of improving the accuracy of these estimates, and consequently improve the predictions of how much melting glaciers and ice caps will contribute to sea level rise in the future.

Table 1: Observed contributions to GMSL, values in mm/yr. (Modified table from IPCC, Church et al. 2014.)

Source	1993-2010
<i>Observed contributions to global mean sea level (GMSL) rise</i>	
Thermal expansion	1.1 (0.8 to 1.4)
Glaciers outside Greenland and Antarctica	0.76 (0.39 to 1.13)
Glaciers in Greenland	0.10 (0.07 to 0.13)
Greenland ice sheet	0.33 (0.25 to 0.41)
Antarctica ice sheet	0.27 (0.16 to 0.38)
Land water storage	0.38 (0.26 to 0.49)
<i>Total of contributions</i>	2.8 (2.3 to 3.4)
Observed GMSL	3.2 (2.8 to 3.6)

Accessing Styggedalsbreen is easy during the summer and early fall. Hydro Energi uses the melt water from Styggedalsbreen to feed hydroelectric power plants in Fortun, and has constructed a dirt road which leads to within 1.5 km from the glacier front. Little previous research has been done on Styggedalsbreen, but NVE (Norges Vassdrag og Energidirektorat) have been recording length change measurements on many glaciers in Jotunheimen, including Styggedalsbreen, since 1901. The general trend is a steady decrease in length over the last 100 years, with the glacier front having retreated as much as 562 m from 1901 to 2013. The early 1990s (89-95) had very high winter precipitation, and as a consequence most Norwegian glaciers experienced an increase in length (Nesje et al. 2008). At Styggedalsbreen a 16 m length increase occurred during this period, but since then there has not been any consistent growth, and from 1997-2013 Styggedalsbreen retreated 105m (NVE: Length change measurements of Styggedalsbreen).

In this thesis we use ground penetrating radar (GPR) measurements of ice thickness from which we can make a relatively accurate estimate of the volume of Styggedalsbreen. The GPR measurements provide radargrams that show several reflections, including glacier bed, and by

interpreting these radargrams we can find the ice thickness of the glacier along each profile. The ice thickness is then subtracted from the digital elevation model (DEM) (Kartverket, 2014) to produce a map of the subglacial topography.

2 Study Area

2.1 Location

Styggedalsbreen is located in Styggedalen in western Jotunheimen (figure 1), a mountainous area containing several glaciers and some of the highest mountains in Northern Europe. Styggedalen is a relatively small valley, extending from the end of Helgedalen in the west, towards Gjertvassdalen in the east. The area is part of “Hurrungane”, well known for its many alpine peaks and sharp arêtes. Large parts of western Jotunheim, including our study area, is located in the municipality of Luster in Sogn & Fjordane County. Glaciers in Norway cover an area of approximately $2692 \text{ km}^2 \pm 81 \text{ km}^2$ (Andreassen et al. 2012), and glaciers in Jotunheimen represent about 10% of this area (Askheim and Thorsnæs, 2014). Of the total area of Norway, glaciers cover approximately 0.7 % (Andreassen et al. 2012).



Figure 1: Overview of Styggedalsbreen (Bygdin 2008)

To illustrate the area, and work done on the glacier, the Bygdin 2008 and Sogn 2010 aerial photos supplied by www.norgebilder.no were used.

Styggedalsbreen extends approximately 2.5km northwards from the northern base of “Styggedalstindane” and “Skarstølstindane”, a range of peaks circling the southern end of the glacier (figure 1). The surface area of the glacier is about 1.85 km² and the average width of the glacier in the region where we conducted the measurements is 442 m (Fylkesatlas (2014)).

The maximum and minimum elevation of the glacier is 1785 and 1295 m above sea level (m .a.s.l.) respectively (Norgeskart 2014, figure 2). There is one outlying arm of the glacier on its southwestern side and several smaller ice fields that are connected to the southern area through icefalls that reach altitudes of 2200 m a.s.l. and more (figure 1). The steep ice fields

above the southern part of the glacier are possibly remnants of an old and much larger Styggedalsbreen.

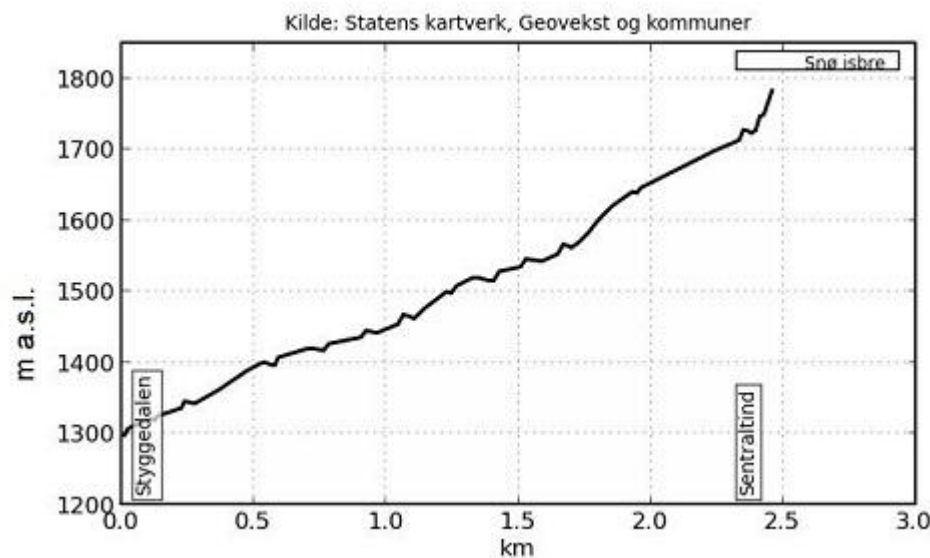


Figure 2: Elevation profile. Generated by www.norgeskart.no

2.2 Glacial features

Styggedalsbreen is a temperate valley glacier with a steep cirque-shaped accumulation area. The large area at the southern end of the glacier is located within a bowl and feeds the part of the glacier moving northwards into Styggedalen. During fieldwork in August / September 2013, patches of firn started to appear at about 1550 m a.s.l., which suggests that the altitude of the equilibrium line (ELA) is located in this region, and that the entire southern area is situated

within the accumulation zone. Area 1 and 2 are below 1550 m and are therefore located within the ablation zone (figure 3).

The surface of the glacier is fairly gentle, with four relatively flat regions (area 1-4, figure 3) separated by steeper and moderately crevassed areas. Measurements were conducted within areas 1-3 in figure 3, while the southern area was considered to be too dangerous due to its close proximity to the surrounding steep terrain and hence an increased risk of avalanches.

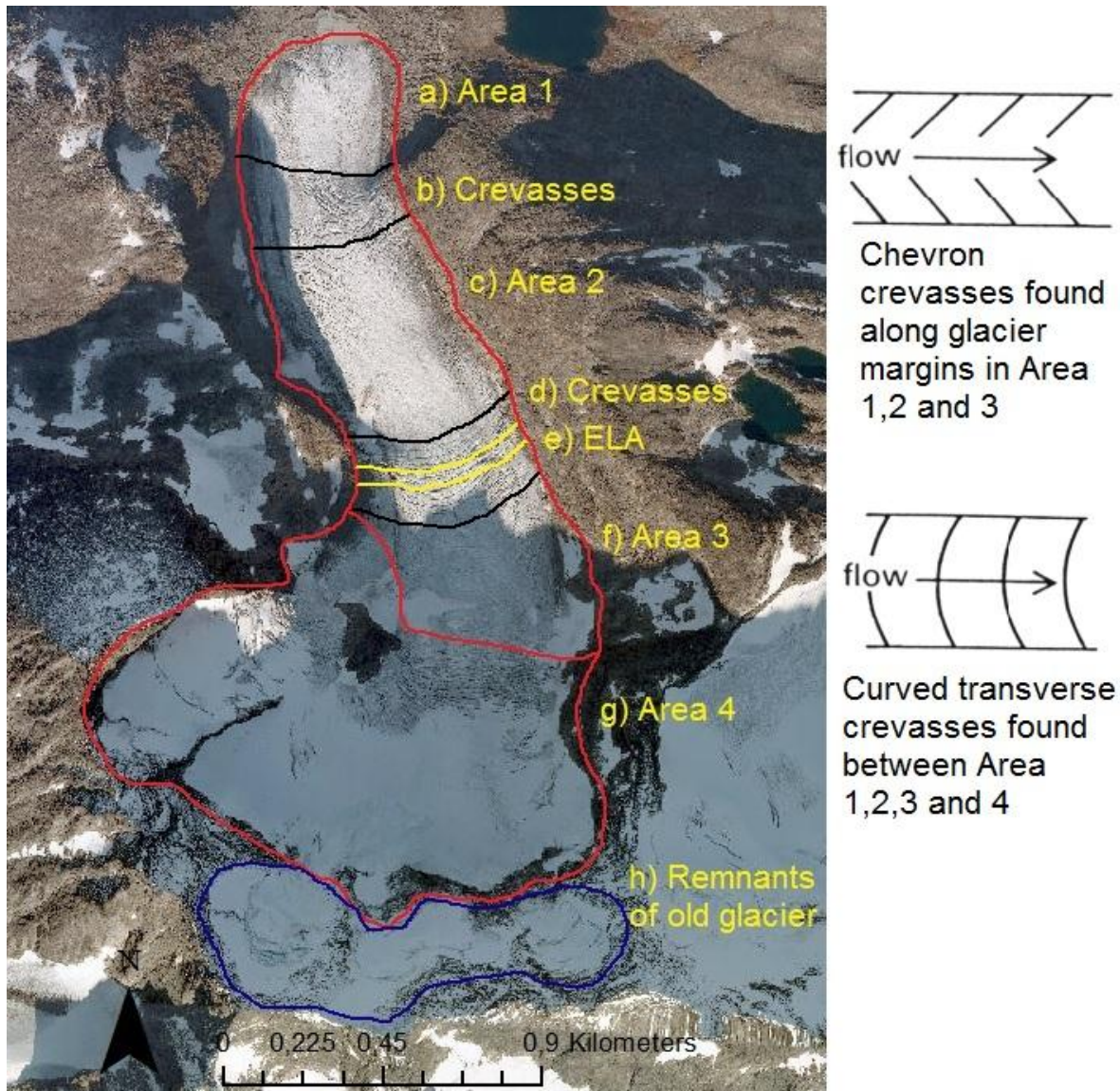


Figure 3: a) Northern flat area. b) Crevasses between area 1 and 2. c) Middle flat area. d) Crevasses between area 2 and 3. e) Approximate location of ELA. f) Southern flat area. g) Area 4 deemed too dangerous to enter. h) Steep ice fields surrounding area 4 (Benn and Evans, 2010) (Bygdin 2008) .

The chevron crevasses at the margins of the glacier are angled towards the centreline and in a southerly direction (figure 3). This type of crevasse is typically associated with drag along the valley walls (Benn and Evans, 2010), and is prominent in area 1, 2 and 3. Another type of crevasse is found in the steeper parts of the glacier, between the 4 plateaus. These curved transverse crevasses open at right angles to the centreline in regions of extending flow, but are curved with the direction of flow when affected by drag from the valley walls (figure 3, Benn and Evans, 2010).

Rock fall debris, ranging in size from pebbles to large boulders, is spread out along the glacier margins. Debris is more abundant on the western side, reflecting the greater steepness of the valley wall compared to the eastern side of the glacier. A supraglacial layer of debris can have a large impact on ablation rates, depending on thickness and density of the layer (Benn and Evans, 2010). Layers of 2 cm or thinner generally have a heating effect, increasing ablation due to the lower albedo of rocks and sediments absorbing more light, which then becomes energy available for melting. Thicker layers have an insulating effect due to the layer acting as a thermal barrier between the ice and the atmosphere, preventing the transport of energy to and from the ice (Benn and Evans, 2010). Even though the amount of debris is considerable at Styggedalsbreen, it is unlikely that it has a large effect on ablation season melting. The large grain size and low density of the debris layer does not create the insulation effect needed to preserve ice during the ablation season or the heating required to increase ablation over large areas. There are scattered pieces of debris located along the centreline of the glacier. Some of these are likely just remains from rock falls that have reached the maximum fallout length, while others are rocks that have resurfaced below the ELA after having been transported internally in the glacier. There is a small medial moraine where the ice flow from the south-western arm meets the main glacier (figure 1). The moraine stretches approximately 500 m north, and contributes to the amount of debris along the western margin.

There is a small proglacial lake at the glacier front that appears to have a depth of approximately 1-3 m (figure 1). It is possible that there is ice beneath the lake and the surrounding glacial sediments, and so the glacier might extend further north than the visual front. Confirming this was not possible due to time and equipment constraints.

2.3 Climate

The climate of Jotunheimen is characteristic of high-mountain regions; temperature decreases as altitude increases, wind is generally more powerful than in the lowlands, most fall and winter precipitation come in the form of snow, and the summers are relatively wet (Barry, 2005).

Using historical weather data from the Norwegian Meteorological institute

(www.eklima.met.no), we are able to get an impression of the overall weather situation near Styggedalsbreen over the last 90 years. The weather station closest to the study area is located at Fanaråken, a 2068 m high peak on the opposite side of Helgedalen, 3.5 km from the glacier front. Climate data is recorded in 30 year intervals to be able to calculate a trend, and as we are nearing the end of the 1991-2020 interval, graphs for this period are not yet available. Instead, we can use data from the 1931-1960 (figure 4a) and 1961-1990 (figure 4b) intervals and compare this to annual data from the last 24 years. Fanaråken weather station has been inactive since 1978, and was only reactivated in 2012. Because of the large data gap, we compared observations from the station at Fanaråken and the station at Sognefjellshytta (1400 m a.s.l.). Sognefjellshytta is located about 7.2 km north-east of Fanaråken and 10.7 km north-east of Styggedalsbreen. When taking into account the difference in altitude, there is still a trend towards higher temperatures, especially in the winter, at the end of the 1990s (figure 4). From looking at the graphs there also seems to be a trend towards more winter precipitation and less spring/summer precipitation (figure 4).

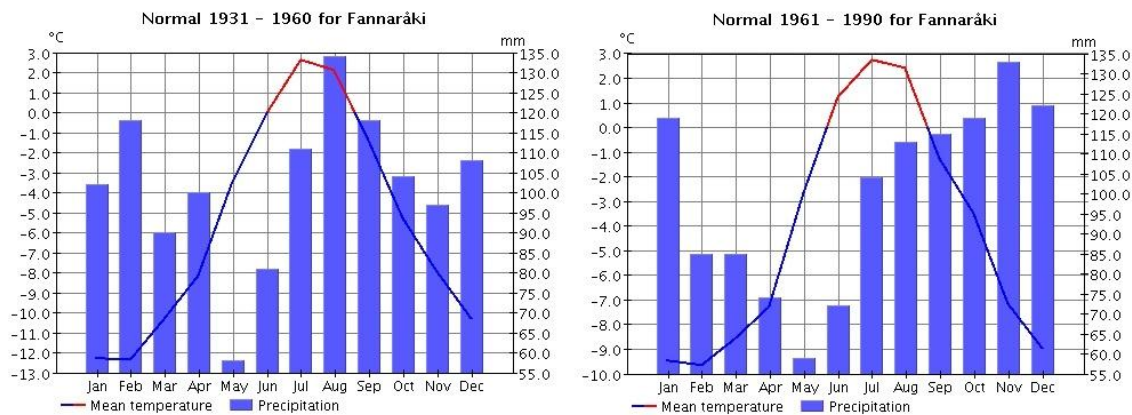


Figure 1: Mean temperature and precipitation for the 1931-1960 a) and 1961-1990 b) intervals. Generated by eKlima.

Wind speed and direction have an impact on the accumulation of snow, which directly impacts the creation of new ice. Since Styggedalsbreen is a valley glacier, it is more protected against strong winds than other, more open, glaciers. The valley walls shelter the glacier from eastern and western winds, while the mountain range to the south deflects much of the southern wind. Most of the wind in the area is coming from west/south-west and south-east (figure 5), and the glacier is well sheltered against incoming winds. Westerly and easterly winds might blow snow from the top of the valley sides and onto the surface of the glacier, adding to the accumulation of snow. Winds coming from the north will be channelled into the valley and follow the glacier surface until it hits the southern rock wall (figure 1), effectively transporting snow from the ablation to the accumulation area.

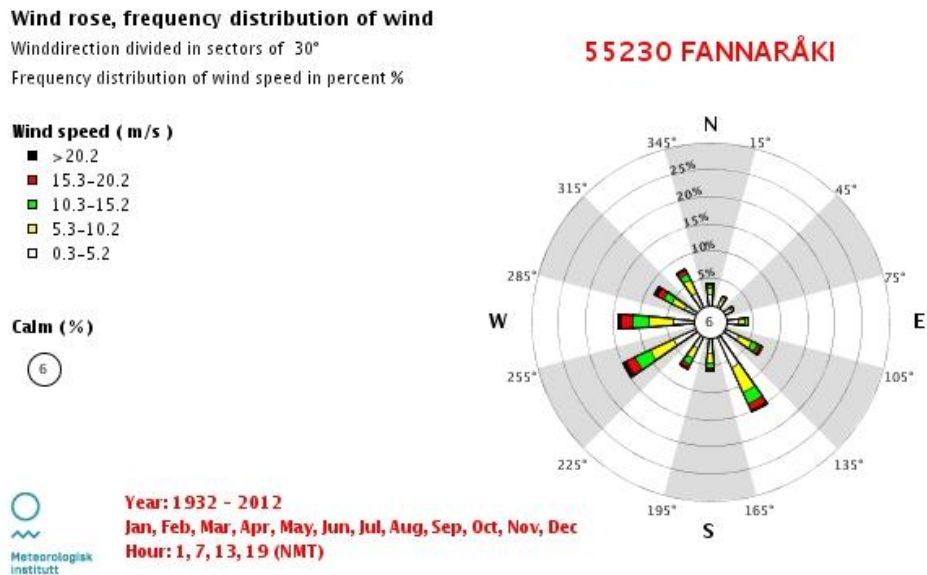


Figure 2: Wind direction and speed at Fannaráken. Generated by eKlima.

2.4 Geology

The bedrock in the area surrounding Styggedalsbreen is mostly gneissic pyroxene granulite, with fields of amphibolite and pegmatite to the east and west of the glacier (*Bedrock geology-N250 Raster map*, 2014). Most of the bedrock in Jotunheimen is part of “Jotundekket”, a thick overthrust sheet of metamorphosed Precambrian igneous rocks which was originally located several hundred kilometres north-west of today’s location, and subsequently slowly thrust

south-east during the Caledonian orogeny (Bryhni, 2011). “Jotundekket” is more resistant to erosion and weathering than the surrounding bedrock, and form the highest mountains in Scandinavia. The many ice ages over the last 2.6 million years have left their mark on Jotunheimen, effectively shaping the alpine landscape through glacial erosion.

The steep valley sides make the area prone to rock falls and snow avalanches, as is evident by the large amount of debris found on Styggedalsbreen’s surface. The southern rock wall has an inclination of 40-60° (figure 6), with some parts being nearly vertical. There is also the danger of ice falling from the higher ice fields and dislodging rocks or larger ice blocks, effectively causing a chain reaction which could lead to a larger event.

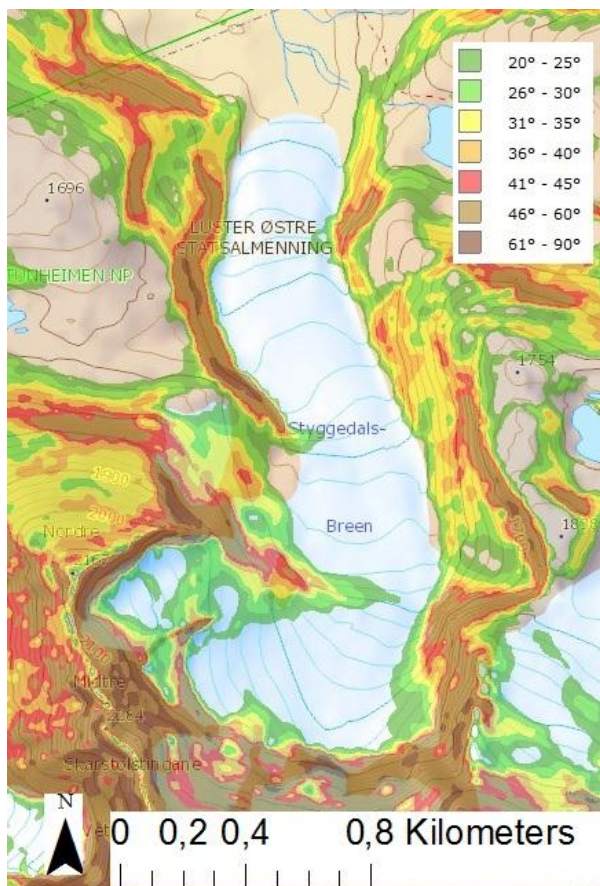


Figure 3: Inclination (www.ngu.no)

The many moraines in front of Styggedalsbreen provide evidence of the way in which the glacier has gradually retreated over the last centuries, with each moraine marking a period of growth or stand-still. The curved end moraines follow the main flow direction of the glacier, turning slightly westwards approximately 500 m north of the glacier front (figure 7). The lateral moraines consist of much coarser material than the end moraines, reflecting the distribution of debris on the glacier surface. With most coarse debris from rock falls being located along the margins of the glacier, this material would be deposited in the lateral moraines as the glacier

retreated. The yellow line on figure 7 marks the Little Ice Age (LIA) moraine, and shows where the glacier front was located around 1750. Over the last 250 years, the glacier has retreated more than 800 m, 560 of which disappeared in the last century alone (NVE: Length change measurements of Styggedalsbreen).



Figure 4: Lateral and end moraines marked in red. The LIA moraine is marked in yellow (Bygdin 2008).

3 Methodology

3.1 Introduction

For the study of Styggedalsbreen, a GPR setup with a 50 MHz and 100 MHz rough terrain antenna (RTA) was mainly used. The GPR is produced by MALÅ Geoscience (Sweden), and is used in combination with a transmitter antenna emitting electromagnetic (EM) waves and a receiver antenna registering reflected waves. The separation between the transmitter and receiver is fixed at 4 meters for the 50 MHz antenna and 2 meters for the 100 MHz antenna. The RTA, the monitor and the ProEx control unit weighs about 14 kilos altogether, which makes it a light and compact GPR system (Malå operating manual v. 2.0) and ideal for use in a supraglacial environment (MALÅ Geoscience, 2011a, Figure 8).



Figure 8: Application of GPR during the accumulation season (A) and ablation season (B), with a 50 MHz and 100 MHz antenna respectively.

3.2 Principle of ground penetrating radar

GPR utilises the transmission and reflection of electromagnetic waves in order to detect and map buried structures. Antenna frequencies range from 1 to 1000 MHz (Annan, 2001; Plewes and Hubbard, 2001.). The transmitter antenna sends out electromagnetic pulses with a certain centre frequency, in our case 50 MHz and 100 MHz. As this energy is conducted through materials in the ground, it will eventually be reflected back to the antenna or absorbed. When the pulsating waves meet boundaries between materials of different properties, they behave differently by increasing or decreasing their velocity. This is due to differences in relative electrical permittivity and electrical conductivity (explained in section [3.3.2](#) and [3.3.1](#), respectively). The waves are reflected at the interfaces and registered by the receiver antenna (figure 9).

The GPR emits electromagnetic waves in all directions from the transmitter antenna. When a current passes through a wire or a coil, it produces a magnetic field. GPR uses alternating current (ac), flowing first one way and then the other. This produces alterations in the magnetic field and causes a series of waves to spread out from the transmitting antenna which the ac passes through. These waves are part of the electromagnetic spectrum, such as x-rays, infrared rays and light, only with different wavelengths (Musset and Khan,2000).

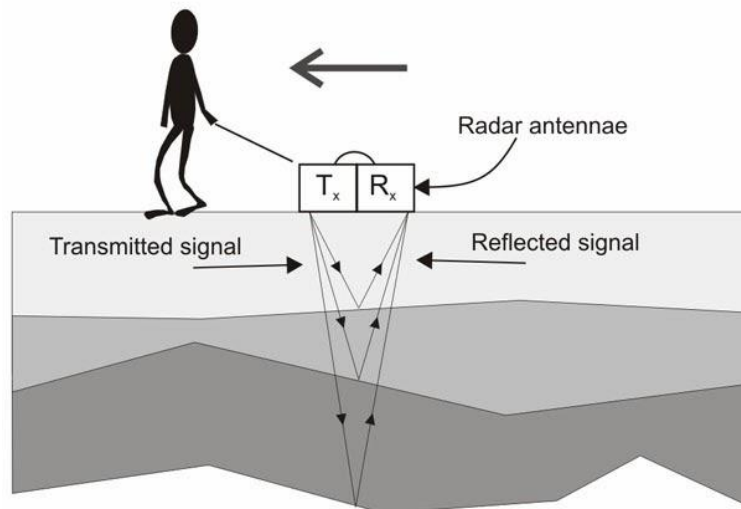


Figure 9: Principle of GPR. Receiver antenna R_x and transmitter antenna T_x are moved over the surface together. Electromagnetic waves are emitted into the ground, - reflected by boundaries and registered by a receiver antenna (Gidusko, 2014).

Not all of the energy is reflected, as some energy will continue through the “new” material with a different velocity and be diverted at a new angle from its original path by refraction. If the ground consists of a homogenous medium, there will be no reflection or refraction as the wave will travel with a constant velocity at a certain angle. The ground has to be heterogeneous,

meaning that it consists of materials with different properties, in order for the waves to be reflected. Although refraction is an important part of wave propagation in different mediums, it is not that relevant to our study. This is because we use a two-layer model, with ice above the glacier bed. We are therefore interested in the reflected waves at this boundary in order to map the bed topography.

3.3 Properties of materials

Two electrical properties control the propagation of radar signals in ice, these are relative electrical permittivity (ϵ_r) and electrical conductivity (σ).

3.3.1 Electric Conductivity

The electric conductivity (EC, microsiemens per meter) of a material describes the ability of that material to conduct an applied electrical current. In GPR surveys, increased radar wave attenuation is primarily related to increased conductivity.

Conduction through atoms will cause the electrons to shift position relative to their nuclei; EM energy used to shift their position will be converted into heat and transmitted to the surroundings, the energy is lost from the propagating wave (Hubbard and Glasser, 2005; Brandt, 2001).

For this thesis the focus is on ice, which has an EC of approximately 0.01 mS/m (table 2). This value is mainly controlled by the degree of impurity (ionic) of the ice, often controlled by sea salt and volcanic deposits, but also by temperature and pressure (Plewes and Hubbard, 2001). Compared to other materials with a high amount of ionic content (sea water and clays, table 2), ice generated from precipitation and freshwater has, in general, very small amounts of ionic content, and thus very low EC (Table 2). Salt water has a very high EC (Table 2) due to its ionic content (NaCl) and impurity. Fresh water, in comparison, has a very low EC, but greater than distilled water. This is primarily due to impurities and natural pollutants. Natural polar ice is therefore more conductive than temperate ice where the impurities are removed (Plewes and Hubbard, 2001). Despite this, electromagnetic waves will penetrate deeper in polar (cold) ice than in temperate ice because of the loss of energy as the waves encounter liquid water in temperate ice.

3.3.2 Relative Permittivity

Electrical permittivity describes the capacity of ice (or any other material) to store an electrical charge. The permittivity is an important part of the propagating velocity of waves given by (Hubbard and Glasser, 2005):

$$V = \frac{c}{\sqrt{\left(\frac{\epsilon}{2}\right)[(1+P^2)+1]}} \text{ Equation 1}$$

Where c is the speed of light ($3 \times 10^8 \text{ ms}^{-1}$), ϵ is permittivity and P is the loss factor defined by $P = \sigma / \omega \epsilon$, where ϵ is electric conductivity and ω is the angular frequency (equal to $2\pi f$, where f is the frequency of the electromagnetic waves emitted by the antenna, Hubbard and Glasser 2005).

The permittivity ($\epsilon, \text{ Fm}^{-1}$) is often related to permittivity in vacuum ($\epsilon_0, 8.854 \times 10^{-12} \text{ Fm}^{-1}$) by this formula (Brandt, 2007):

$$\epsilon_r = \frac{\epsilon}{\epsilon_0} \text{ Equation 2}$$

ϵ_r is referred to as the relative permeability, commonly called the dielectric constant (Hubbard and Glasser 2005).

Since the electric conductivity in ice is very low and the frequency is not fixed we use a simplified version of equation 1, given by the speed of light and the relative permittivity (ϵ_r , equation 1) in the equation (Hubbard and Glasser, 2001):

$$\epsilon_r = \left(\frac{c}{v}\right)^2 \leftrightarrow V = \frac{c}{\sqrt{\epsilon_r}} \text{ Equation 3}$$

For ice, the relative permittivity is relatively low (~3) in comparison to that of water (80, Table 2). Ice with high water content will therefore affect the penetrating wave.

The relative permittivity of the ice itself will be affected by crystal orientation, density and purity, all to a different extent.

3.3.3 Velocity and depth calculation

The velocity of EM waves through a material is mainly influenced by the permittivity of the ground (or the material), but is also to a lesser extent controlled by electric conduction and the radar wave frequency, as mentioned above (Hubbard and Glasser, 2005). Velocities of electromagnetic waves in different mediums are shown in table 2.

Table 2: Electrical properties for different materials. Modified from Plewels and Hubbard (2001), Erlend Førrre (2012) and MALÅ Geoscience (2011a).

Material	Relative electrical permittivity (ϵ_r)	Electrical conductivity (σ) (mS m^{-1})	Velocity (V) ($\times 10^8 \text{ ms}^{-1}$)	Attenuation (α) (dB m^{-1})
Air	1	0	3.0	0
Distilled water	80	0.01	0.33	0.002
Fresh water	80	0.5	0.33	0.1
Salt water	80	3000	0.1	1000
Clay	4-40	2-1000	0.6	1-300
Granite	4-6	0.01-1	1.3	0.01-1
Polar snow	1.4-3	-	1.94-2.52	-
Polar ice	3-3.15	-	1.68	-
Ice	3-4	0.01	1.50-1.73	0.01
Permafrost	4-8	-	1.06-1.50	

Velocity in ice is given by the rearranged equation 3.

Measurements of the velocity of radar waves in ice have been done both in the field and in laboratories, and have given an approximate velocity of $1.67 \times 10^8 \text{ ms}^{-1}$ (Hubbard and Glasser, 2005). This value differs depending on the type of ice the EM waves travels through: the velocity is slightly higher in cold and dry glaciers (maximum $1.73 \times 10^8 \text{ ms}^{-1}$, table 1) and lower in temperate glacier with higher water content and warmer ice ($1.50 \times 10^8 \text{ ms}^{-1}$, table 1). In the case of this study, the surveys were made on a temperate glacier with relatively high water content. During the accumulation season the ice is protected by a layer of insulating snow, keeping the glacier ice relatively warm.

During the ablation season there will be much supra-, en-, and subglacial water because of melting, and precipitation usually takes the form of rain. Field measurements suggest a large span of velocities in ice due to the water densities and air pockets (Bradford and Harper, 2005). This is because of the large difference in velocity between ice, water and air which has values of $1.67 \times 10^8 \text{ ms}^{-1}$, $0.33 \times 10^8 \text{ ms}^{-1}$ and $3 \times 10^8 \text{ ms}^{-1}$ respectively.

When the velocity is determined and the “two way time” (TWT) of the registered EM waves are recorded, we can calculate the depth to reflections and boundaries. This can be at the

boundary between ice and water, or more relevant to our study; between ice and bed. The depth is given by a formula (Plewes and Hubbard, 2001):

$$d = \frac{TWT * V_{ice}}{2} \text{ Equation 4}$$

3.4 EM wave propagation

The loss of radar signal strength in ice is caused by a number of processes, such as: geometrical spreading, attenuation, scattering and absorption (Hubbard and Glasser, 2005). These are all summarized in figure 10:

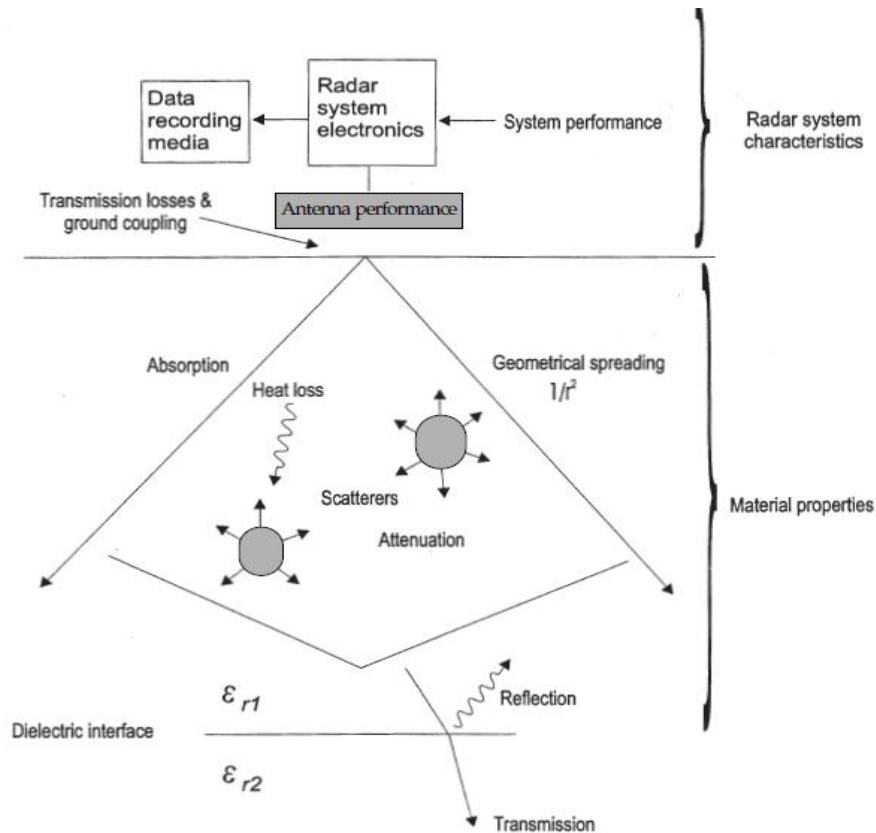


Figure 10: How a GPR system is characterized and the propagation of electromagnetic waves. Modified after Plewes and Hubbard (2001).

The loss of signal is expressed in terms of the skin depth, which is referred to as the distance in meters to which the signal strength has decreased by about 37% or 1/e (e is the exponential, 2.718, Hubbard and Glasser, 2005). The skin depth is given by the equation (Mussett and Khan, 2000) :

$$\text{Meters (depth)} = 500 \sqrt{\frac{1}{\sigma f}} \text{ Equation 5}$$

In glaciological studies, this equation is mainly controlled by the frequency since the conductivity is usually low in ice (and in other mediums, table 2). This implies that radars with a relatively low centre frequency will have a much larger penetration depth than that of an antenna with a higher frequency. The radar signal attenuation is positively related to the signal frequency, resolution is therefore often preferred over penetration (Plewes and Hubbard, 2001). In our study, the penetration was preferred over resolution because we wanted to detect the boundary between ice and bed, and not structures in the ice.

The degree of details the radar can produce is defined as the resolution. The better the radar system, the better the resolution and the more accurately it can reproduce sizes and shapes of reflectors (Hubbard and Glasser, 2005). Although the resolution decreases with lower antenna frequency, the loss of wave energy in a glacier is low compared to that in soil or bedrock like clay and granite (table 2). This means that a high frequency antenna can detect relatively deep buried structures. This is of course relative to the depth of the glacier and the numbers of reflectors present (water content, crevasses, rock etc.). For this study the 50 MHz antenna was preferred as it gave better results for the deeper parts of the glacier.

3.4.1 Attenuation

The signal is attenuated when penetrating the ground due to a number of processes, including; scattering, absorption and geometrical spreading (figure10). Signal attenuation includes all of these variables and describes the loss of signal strength (dB). The signal attenuation coefficient (α) describes the loss of energy per meter travelled (dBm^{-1}). In ice, α is relatively low and thus results in a high penetration depth (table 2). Attenuation in ice will differ as the ice is not always homogenous, and therefore the values of relative permittivity and conductivity will vary.

3.4.1.1 Scattering

Much of the signal strength is lost due to scattering of waves, meaning energy loss due to processes like reflection, refraction and diffraction (Hubbard and Glasser, 2005). Reflection is what we need in order to locate the bottom reflector of Styggedalsbreen. Unwanted scatter is characterised as noise. Dielectric (relative permittivity) and geometrical contrasts in scattering bodies in the ice will enhance energy loss. Scattering losses are a function of the bodies present (numbers, sizes and types) and increases with increased antenna frequency (Hubbard and Glasser, 2005).

3.4.1.2 Absorption

Two processes are mainly responsible for the absorption of EM waves in ice: relaxation and conduction. Relaxation is defined as the oscillation of water molecules; this will cause the EM

waves to lose energy. Through conduction the EM energy is lost to the surroundings as heat (see section [3.3.1](#))

3.4.1.3 Geometric spreading

Geometric spreading occurs as the radar waves are transmitted away from the antenna (figure 10). The energy will spread out and be subjected to geometric spreading with a rate of $1/r^2$, where r is the distance travelled from the point of origin (Plewes and Hubbard, 2001).

3.4.1.4 Reflection

When an EM wave meets an interface it will scatter the energy according to three parameters: 1) the shape and roughness of the interface, 2) the contrast in electrical properties (ϵ_r and less important, σ) between the host media and the object which it encounters and 3) the depth to the target (Daniels, 2000; MALÅ Geoscience, 2011a). The energy is reflected back to the host media or will travel into the object which it encounters.

With reflections directly below the antennas, the wave front change direction at the interface between the two different media and is returned to the point of origin (figure 11). The reflection strength is expressed mainly in terms of the contrast of electric permittivity between the mediums. The contrast in relative permittivity and velocity is given by the reflection coefficient (equation 6), and is the ratio of the amplitudes between the reflected and the incident waves (equation 6, Musset and Khan, 2000).

$$R = \frac{\sqrt{\epsilon_2} - \sqrt{\epsilon_1}}{\sqrt{\epsilon_2} + \sqrt{\epsilon_1}} = \frac{v_2 - v_1}{v_1 + v_2} \text{ Equation 6}$$

Where v_1 is the velocity of the top layer and v_2 is the velocity of the underlying layer.

The law of reflection states that the angle of reflection is equal to the angle of incident (Daniels, 2000).

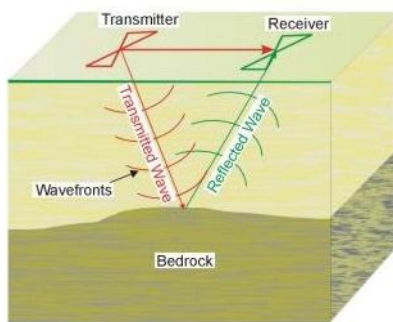


Figure 11: A wave is reflected at the layer boundary. Modified after U.S. Department of transportation.

The part of the wave that is not reflected can be refracted and travel into the object it encounters.

3.4.2 Hyperbolas

Hyperbolas appear as arc-shaped artefacts on radargrams when the GPR registers the presence of a buried discontinuity, which will scatter the radar signal in all directions (figure 12). As the GPR approaches the object, moves over it and eventually passes it, the GPR will register the object as an arc shape because the distance between the object and the GPR decreases, hits a minimum when the antennas are directly above it and then increases again. The arms of the hyperbola thus lead towards the buried reflector located at the top centre of the arc. When processing radargrams, hyperbolas can be removed by folding the arms back towards the top centre of the arc through a process called migration (Plewes & Hubbard, 2001). Hyperbolas in glacial radargrams are often signs of crevasses, buried rocks/boulders, or englacial pockets of water.

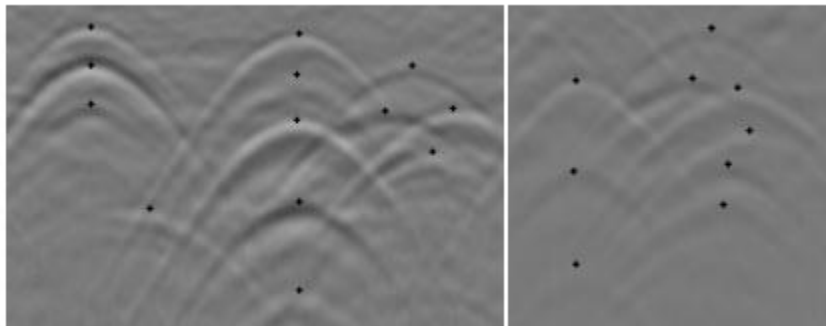


Figure 52: Hyperbolas with the actual reflector/object marked in black. Modified after Birkenfeld (2010).

Hyperbolas were observed in several profiles during the ablation season surveys (figure 13). What the hyperbolas represent on the GPR profile shown in figure 13 is not known, but it could be englacial meltwater, rocks or boulders.

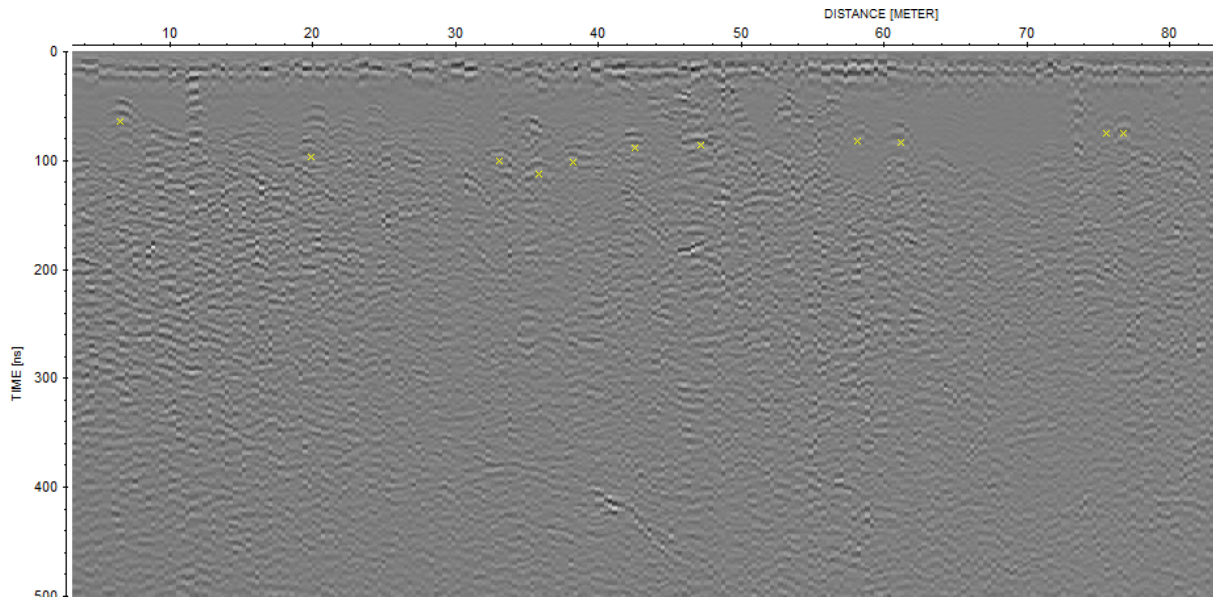


Figure 13: Several hyperbolas in profile 159, marked with a cross underneath. In this radargram the data is only partially processed and the calculated distance has not been corrected.

3.4.3 Side-swipes

When measuring along the margins of the glacier, it is possible for the GPR to register reflections from the valley side below the glacier surface instead of the bed directly beneath. This phenomenon is called side-swipes, and will cause the radargram to show a reflector that is shallower than the actual depth beneath the GPR (figure 14).

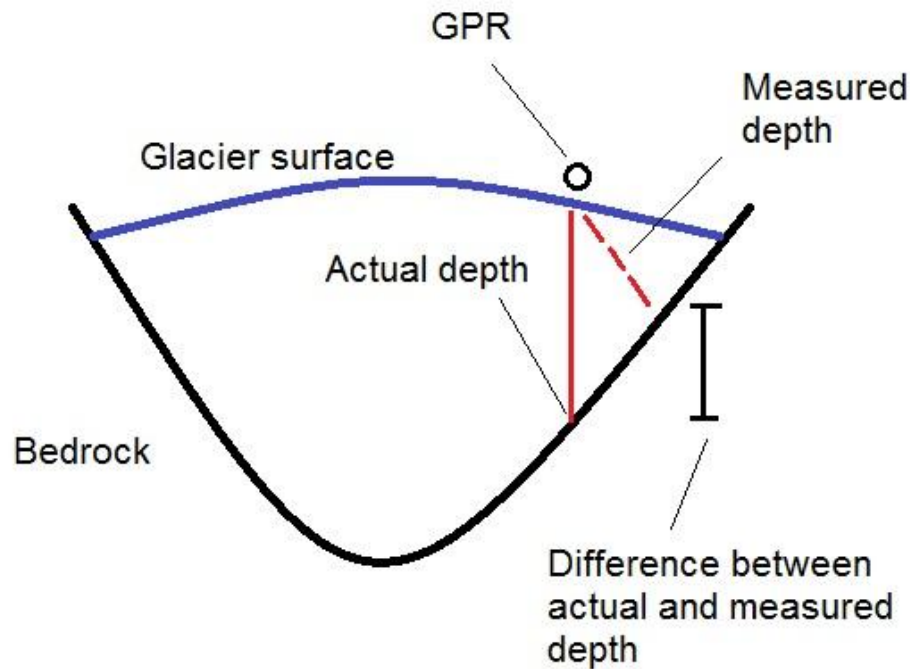


Figure 14: Side-swipe.

3.5 GPR settings

For the first survey in August 2013, we programmed the GPR parameters to match the conditions on the glacier at the time. These setting mostly stayed the same for the 2nd survey in September 2013, but some were changed for the 3rd survey in March 2014.

The antenna is a fixed unit, meaning that the antenna separation is set to a permanent length. For the August/September surveys, a 50 MHz and 100 MHz antenna were used, with an antenna separation of 4 m and 2 m, respectively.

Velocity: velocity is the speed of the EM waves in a given medium. Since the first surveys were done late in the ablation season, we set the velocity to $1.65 \times 10^8 \text{ ms}^{-1}$. This value was chosen because of the high amount of water in the glacier which lowers the velocity of the EM waves. Velocity was not changed for the third survey in March.

Time window: The time window is a value that represents the amount of time the antenna is able to register a reflected signal, before stopping to register to avoid disturbances from other sources. The time window is set to a low value if the expected reflector is shallow and to a high value if it is deep. We set time window to 1198.0 nanoseconds (100.9m penetration depth in ice assuming a velocity of $1.65 \times 10^8 \text{ ms}^{-1}$), this parameter reflects the maximum ice thickness we expected to find on Styggedalsbreen.

Acquisition mode: Acquisition mode was set to time triggering, and the time interval set for the surveys varied between 0.5s and 2.0s. The higher time interval was chosen to preserve the batteries since we did not know how long they would last in low temperatures.

Sampling frequency: Sampling frequency is defined as the number of samples per unit of time along each trace, and reflects the resolution and amount of detail in the collected data. Higher sampling frequency gives higher resolution, while lower sampling frequency gives lower resolution. The sampling frequency should be set at about 10 times the antenna frequency (MALÅ Geoscience 2011), and when using the 50 MHz antenna the frequency was set to 509.0 MHz while we used a value close to 1000 MHz when applying the 100 MHz antennas.

Stack: is the number of samples for each trace the GPR stacks together to find a "mean" trace. This is the trace shown on the monitor. There is an option called Autostack which stacks a number of traces every second, this option uses a lot of power and data storage, however, and should be used carefully. In this survey we used a rate of 8 stacks to preserve batteries, but still get relatively good data.

GPS: Global positioning system (GPS) data was collected using a Globalsat BU-353 usb gps which plugs right into the GPR monitor. The Globalsat GPS connects each trace with a set of x-y-z coordinates which are stored in a .cor file. GPS and GPS-data are discussed in more detail in section [3.7](#).

3.6 Processing of GPR profiles

Processing data is necessary in order to identify the ice-bed interface. Reflex2D-Quick (R2DQ) and RadExplorer were used as data analysis software for the interpretation of the signals registered by the GPR. We started out using mainly RadExplorer as an interpretation program, but we decided to use R2DQ in addition to RadExplorer because of problems adding external GPS data to the measurements. Figures from both programs are used in presenting the results. But the profiles interpreted in R2DQ are the ones used for depth calculations. For interpretation, several processing tools were used in R2DQ:

Static correction: time=0 should be correlated with the first signal. If this is not corrected for, the depth will be wrong as the time to the reflector is wrong. Automatic static correction was applied. This automatically determines the first significant arrival and adjusts the start position of the time axis to this point (Sandmeier, K-J).

Subtract-mean (dewow): Dewow eliminates low frequent displacement of data which is common in GPR. The tool finds the amplitude midpoint for the reflected waves and places them at amplitude equal to 0. R2DQ will automatically set a default value for the time window (Sandmeier, K-J).

Gain function: Gain function amplifies the amplitudes of the signal using linear and exponential functions. The amplification is done to compensate for the possible losses due to damping or geometric spreading (Sandmeier, K-J).

Bandpass butterworth: In this filter band two frequency values are set; these determine the lower and upper cut-off frequencies. This tool attempts to suppress unwanted low and high frequency noise (Sandmeier, K-J).

Background removal: This processing tool is used to eliminate noise in order to try to make signals in a profile more visible (Sandmeier, K-J).

Migration: By migrating the GPR data we account for reflections from points that are not directly below the transmitter (side-swipes), thereby placing the reflectors in the correct positions in the radargram (see section [3.4.3](#)). In studies of glaciers, a migrated east-west profile will have steeper valley sides than a non-migrated profile. Migration was used to process most of the radargrams i, but some profiles were left unmigrated due to a loss of signal strength, making it difficult to interpret.

Figure 15 shows an unprocessed profile (223) in which the x-axis does not show the correct distance. The distance here is calculated from a constant trace-increase (the distance between traces) and the number of traces. Trace-increase set by R2DQ is 4.6, but our calculations (equation 7) set the trace-increase to 3.59, giving a shorter profile distance of 293 meters (figure 15).

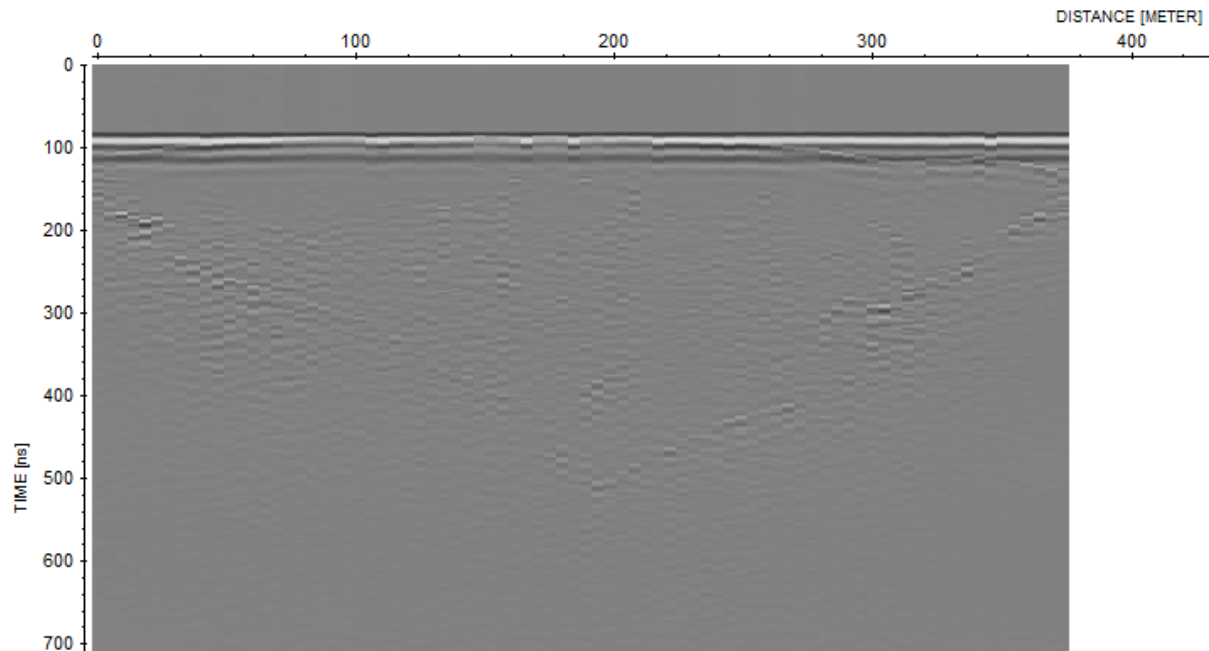


Figure 15: Radargram showing raw, unprocessed data. The y-axis to the left shows the TWT. The x-axis shows the distance in meters.

The processing routine was adapted to best suit each profile, as some profiles showed stronger or weaker reflectors when processed with a certain tool. The processing tools and values used for different profiles are listed in appendix A.

After several steps of processing in R2DQ, we were able to see reflections difficult to detect in the raw data.

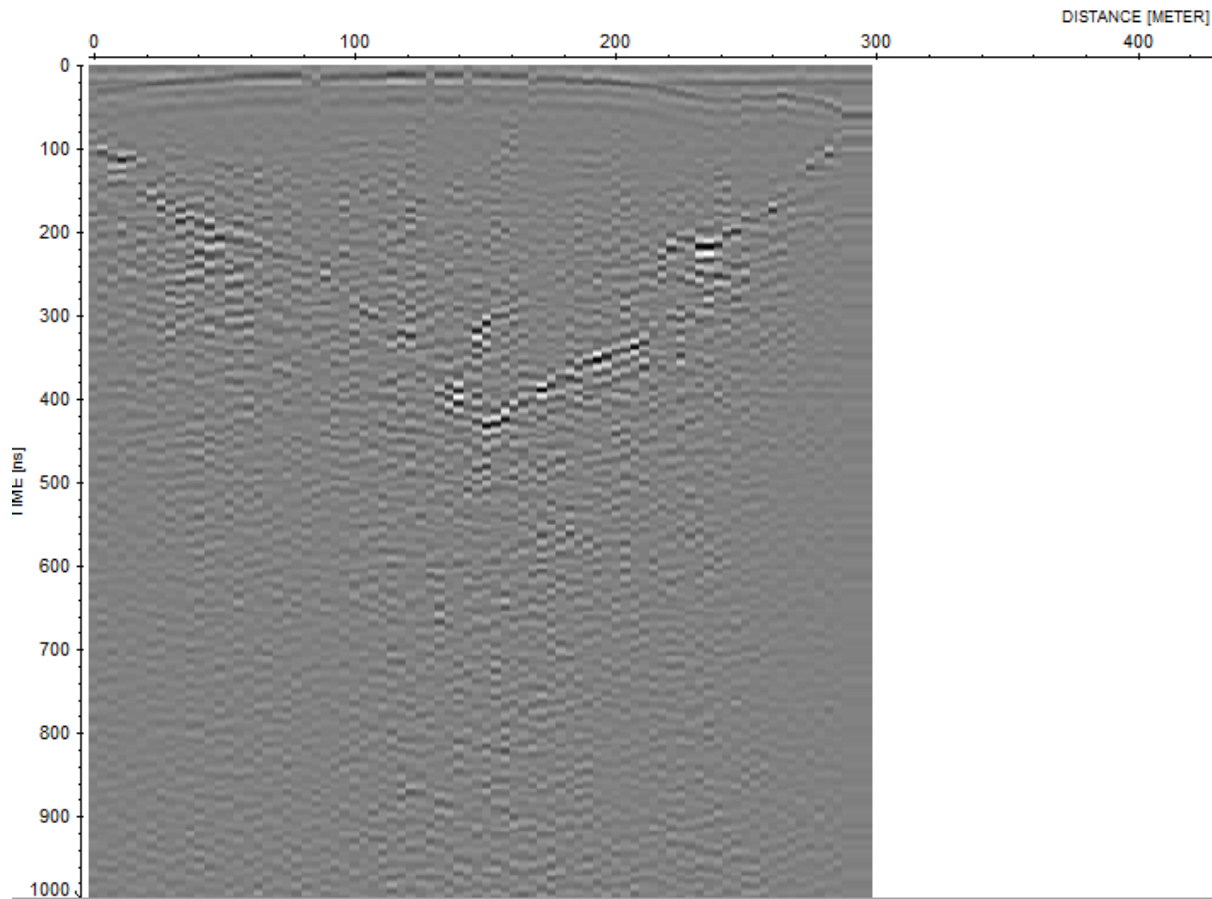


Figure 16: Post processing model. Distance is corrected and the reflections are stronger than in the unprocessed profile in figure 15.

After processing, the GPR profiles were interpreted. A manual picking mode was used to mark promising reflectors and give a clear image of the ice-bed boundary. An interpretation of the subglacial topography along a cross profile is shown in figure 17.

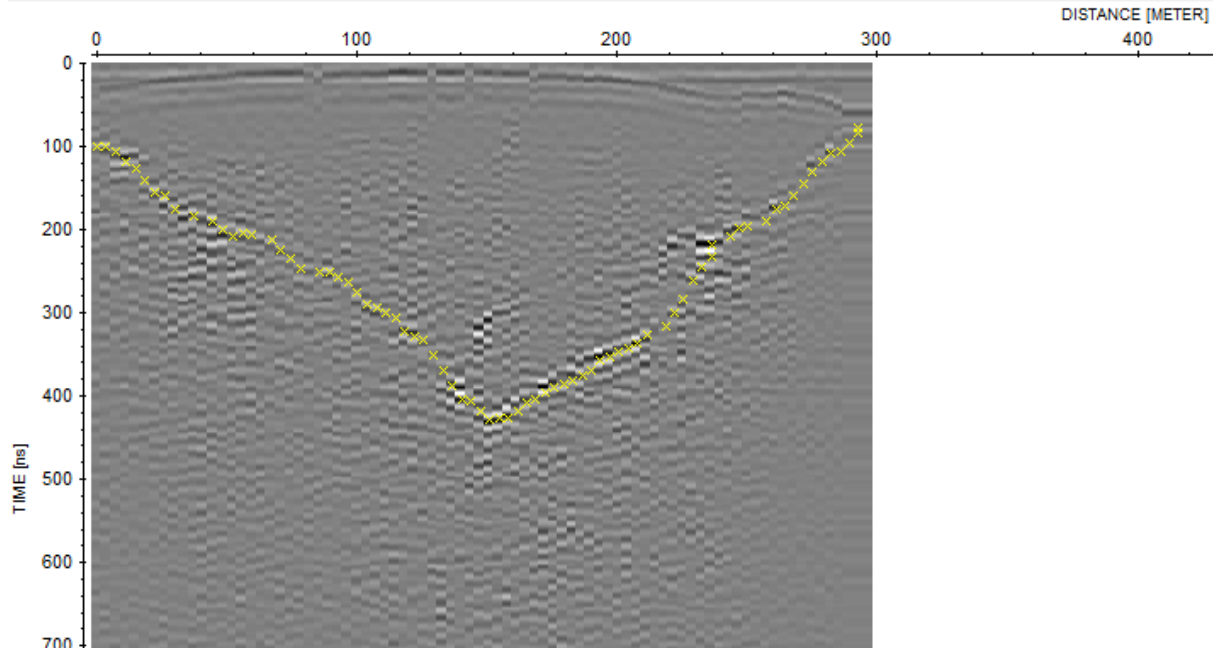


Figure 17: Processed profile with picking for depth calculation.

3.7 GPS data

Connecting the different GPR profiles to a set of GPS coordinates is critical for correctly placing the profiles on a map, locate profile intersections and calculate a volume estimate. By adding depth data from the GPR profiles to a series of GPS coordinates, we can use a DEM in GIS to help model the subglacial topography of Styggedalsbreen.

The Malå GPR unit we used during fieldwork is compatible with handheld USB GPS receivers from GlobalSat. For each trace registered on the GPR, the GPS receiver records a set of X-Y-Z coordinates. This enables us to trace each profile on a map by exporting the GPS data from the GPR and importing it into ArcGIS. This system worked well during fieldwork in August/September 2013. We were able to measure several profiles on the glacier with the GPS receiver recording the corresponding coordinates. As a backup, we were also logging each profile with a normal handheld GPS.

During fieldwork in March 2014, both the GlobalSat GPS receiver and the backup handheld GPS failed for unknown reasons, but fortunately we had a 2nd backup GPS in the form of a GPS watch. However, the watch stored all GPS data as a continuous track on “Google Maps”, and

exporting the data into an excel spread sheet only provided us with the exact coordinates of the start and end of the track, not the movement in between (figure 18).



Figure 68: GPS track made with Suunto Ambit GPS watch shown on “Google Maps”. Generated from www.movescount.com.

This data is not useful in itself, but we can use the Suunto GPS track as a basis to manually draw each profile in a GPS mapping service, and extract the track as a set of X-Y coordinates which can then be imported into ArcGIS. The GPS mapping service we used is called GPSVisualizer (www.gpsvisualizer.com). This online mapping program allows you to draw a track directly onto a map and extract the corresponding coordinates in an excel spread sheet. Using this method we managed to secure a set of X-Y coordinates that match the distance and direction of our profiles. To include Z coordinates in our GPS data we had to manually enter the correct height for each X-Y coordinate. This was done by comparing the new GPS tracks with the similar ones from 2013, which include Z coordinates. Where no previous GPS data existed, contour lines on the toporaster 2 WMS were used. To check the accuracy of the Z coordinates we imported the data into GIS and compared the GPS data with the DEM.

Since GPS data is not included in the GPR profiles from March 2014, we had to manually merge the two datasets in R2DQ. After this was done, we could start interpreting the radargrams. Each trace is then assigned a new set of coordinates (depth) that represent meters from the glacier surface to the ice-bed interface.

To correctly merge the GPR and GPS data from March 2014 in R2DQ, we choose a set of reference points of approximately equal distance from each other along each profile. The corresponding GPS coordinates and trace numbers are input into R2DQ, allowing the program

to calculate the GPS coordinates for the remaining traces through linear interpolation. Because the GPS data from GPSVisualizer does not show a continuous line of coordinates, but rather points along a line, we have to pick among these when choosing reference points. To locate the traces corresponding to these positions we divided the length of each profile with the number of traces recorded. What we find from this is the distance between each trace, which is used to calculate the trace number when knowing the distance from the start of the profile to the reference point (figure 20). This method assumes that the data collection speed is constant.

$$\frac{\text{profile length}}{\text{number of traces}} = \text{distance between each trace Equation 7}$$

$$\frac{\text{distance from profile start}}{\text{meters per trace}} = \text{trace number at reference point Equation 8}$$

An example of an input GPS file used to assign GPS points to GPR traces in R2DQ is shown in figure 19. A conversion from decimal degrees to UTM was done in R2DQ and the correct distances along each GPR profile were then automatically calculated.

	A	B	C	D	E	F	G	H
1	trace number	distance	shot-X-pos	shot-Y	reciever-X	reciever-Y	shot-Z	reciever-Z
2	1	0	7.8802443	61.4880224	7.8802443	61.4880224	1294	1294
3	22	0	7.8788066	61.4878688	7.8788066	61.4878688	1298	1298
4	40	0	7.8775835	61.4877971	7.8775835	61.4877971	1303	1303
5	61	0	7.8761888	61.4877458	7.8761888	61.4877458	1298.5	1298.5
6	82	0	7.874794	61.4877049	7.874794	61.4877049	1292.5	1292.5
7								

Figure19: Input data for R2DQ to calculate correct distances. Excel dataset.

4 Results

4.1 Data collection

During fieldwork in August and September 2013, a 50 MHz and 100 MHz RTA were used to survey the glacier bottom topography. Both antennas were applied because we wanted to see the difference between the two antennas, and because we experienced technical problems with the 50 MHz antenna. The profiles from August and September were of varying quality, with most of them being very difficult to interpret. This was likely due to the limitations of the 100 MHz antenna and the high water content of the glacier. As a consequence we decided to return in March 2014, when the amount of water in the glacier is much lower, and the snow cover enabled us to walk relatively unhindered on the glacier surface.

During the March 2014 fieldwork only the 50 MHz antenna was applied due to its ability to penetrate deeper into the ice. Compared to the profiles made in 2013, the new profiles were of much better quality (figure 21). A total of 10 profiles, 4 in a north-south direction and 6 in an east-west direction, were measured on March 25th 2014 (figure 20). In addition to getting a clearer view of the bottom topography along the east-west profiles, the new measurements gave us a better view of the north-south bottom topography, which was missing in the 2013 profiles.

For estimating the volume of Styggedalsbreen we used one profile from the fieldwork done in September 2013 (profile 159:100 MHz) in addition to 10 50 MHz profiles from the fieldwork done in March 2014 (figure 20).

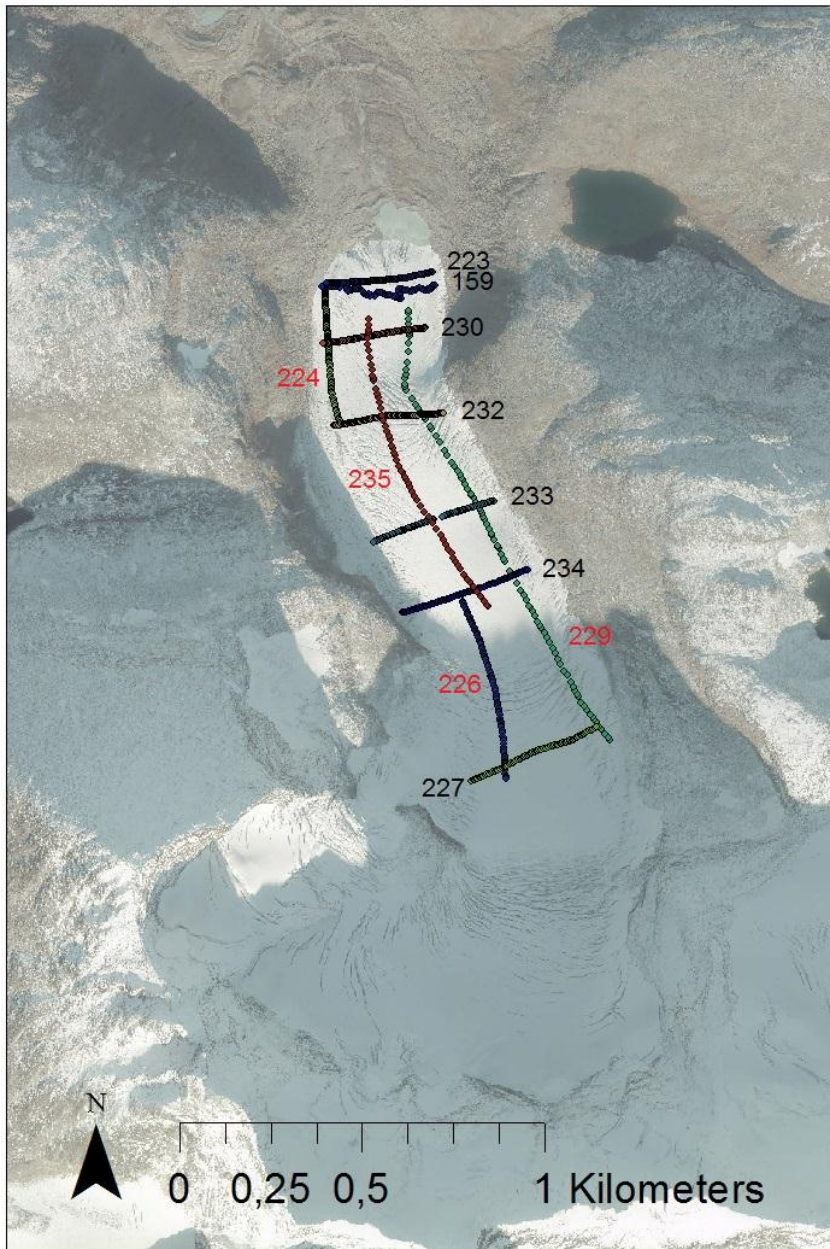


Figure 20: Profiles from March 2014 and September 2013 (159). Red = north-south, black = east-west. Notice the difference between profile 223 and 159 due to snow covering the crevasses.

Profile 159 is approximately the same as profile 223 in terms of distance and location (figure 20), and can be used to show the difference between the 50 MHz and 100 MHz antenna, and ablation and accumulation season.

When comparing profile 223 and 159, we can clearly see the difference between the 50 MHz and 100 MHz antenna (figure 21, figure 22). The bottom reflector, while still visible, is much

harder to make out on profile 159. The 100 MHz antenna provides better resolution and more details, but the 50 MHz antenna is able to penetrate deeper into the ice and gives a more complete image of the bottom reflector as discussed in section [3.4](#).

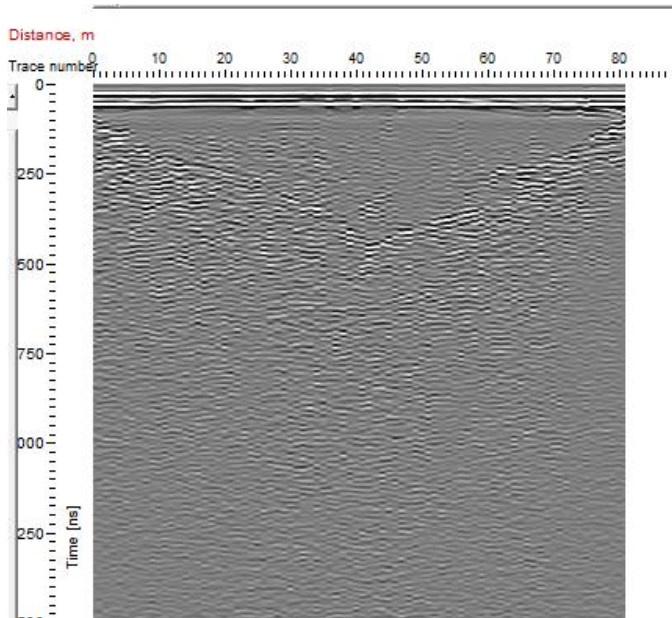


Figure 21: Profile 223 (50 MHz) from March 2014. East-west profile near the glacier front. The curved glacier surface is clearly visible near the top of the profile.

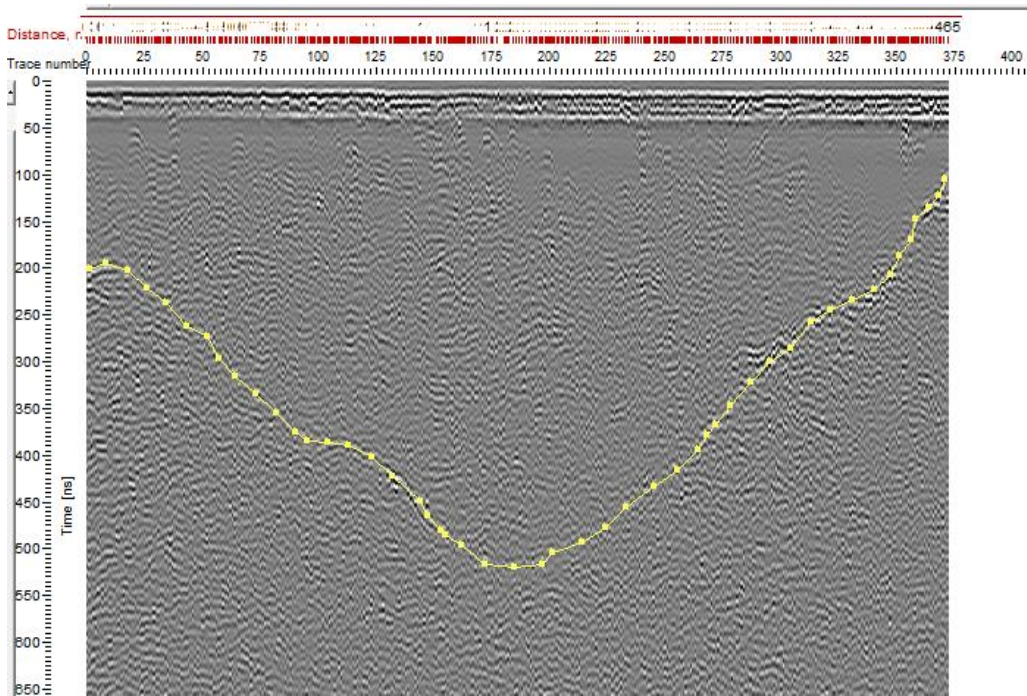


Figure 22: Profile 159 with bottom reflector marked yellow (100 MHz) from September 2013. East-west profile near the glacier front.

4.2 Interpretation

Profile 161 is a typical example of the profiles made in August/September 2013 (figure 23). Even after intensive processing we were not able to extract a definite bottom reflector. Neighbouring profiles were also very difficult to interpret, meaning that we could not use a good profile to “solve” others.

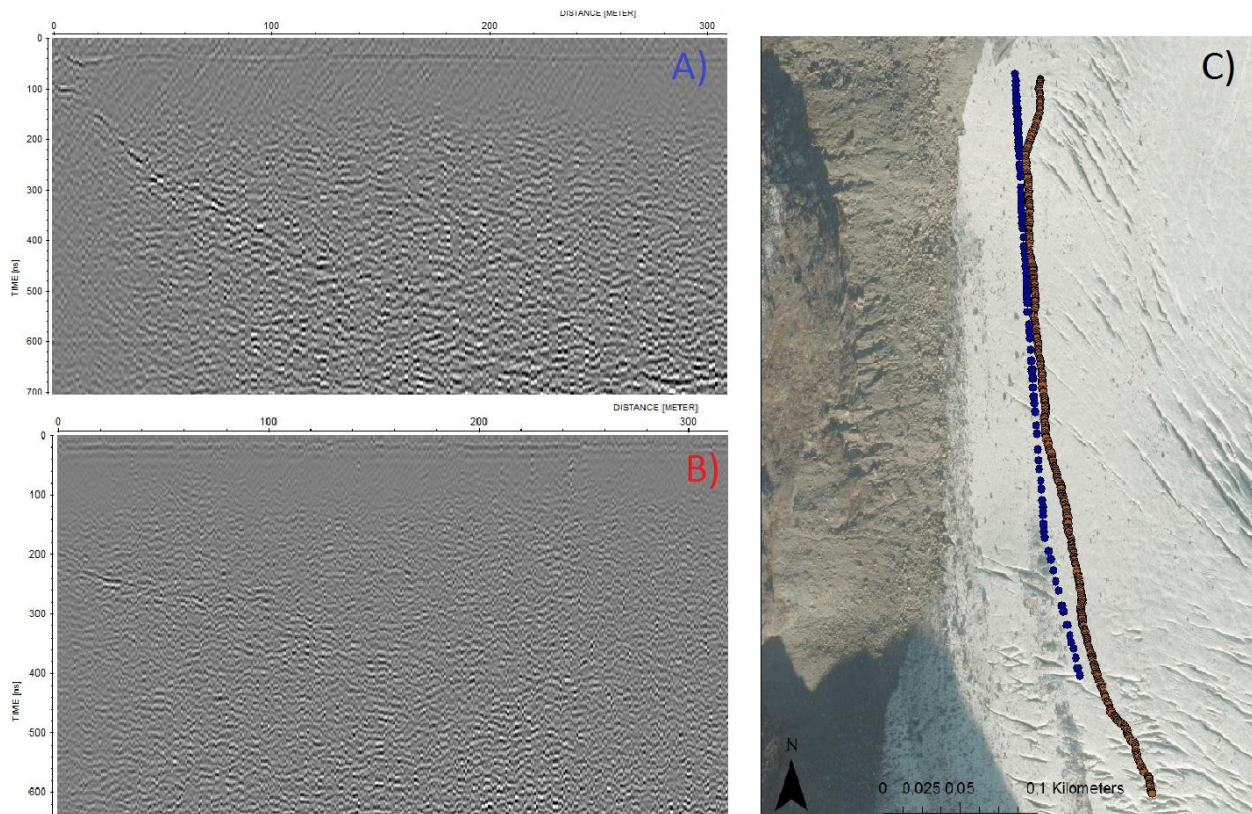


Figure 23: A) Profile 224 measured with a 50 MHz antenna in March 2014. B) Profile 161 measured with a 100 MHz antenna in September 2013. C) Location of profile 224 and 161. Profile A is the blue line and profile B is the red line. The two profiles have undergone processing best suited for each profile.

Profile 224 proved to be one of the better profiles from March 2014 (figure 23A). The bottom reflector is visible along the entire profile, making the interpretation much easier than with profile 161 (figure 23B).

While some profiles were still unclear, interpreting the best profiles first and looking at the intersections enabled us to interpret the more difficult profiles. After having plotted all the profiles in ArcGIS, we were able to evaluate the accuracy of our interpretations by looking at each profile intersection individually and finding the ice thickness difference (table 4).

Table 4: Difference in measured depth between profiles at profile intersections. Margin of error calculated from a mean ice thickness of 28.6 m. (**profile 234 and 226 does not directly intersect, but are offset by approximately 20 meters, *Profile 9 is excluded from the calculated average)

Intersection #	Profiles intersecting	Y coordinate (UTM)	X coordinate (UTM)	Depth difference	Margin of error in %
1	223 and 159	6817629,317974	440124,118957	5,65 m	19,8
2	224 and 230	6817465,666695	440086,488434	2,37 m	8,3
3	230 and 235	6817483,815207	440195,123877	11,49 m	40,2
4	230 and 229	6817502,109285	440308,528043	1,74 m	6,2
5	224 and 232	6817242,052139	440119,505022	0,8 m	2,9
6	232 and 235	6817264,775576	440236,981808	3,08 m	10,8
7	232 and 229	6817268,951507	440344,452452	1,19 m	4,2
8	235 and 233	6816978,811631	440364,11303	10,25 m	35,8
9*	233 and 229	6817020,857649	440497,765647	29,72 m	-
10**	234 and 226	6816775,914785	440447,181033	2,38 m	8,3
11	234 and 235	6816790,59121	440490,800819	3,31 m	11,6
12	234 and 229	6816828,272239	440591,727111	4,38 m	15,3
13	226 and 227	6816305,783528	440571,975635	3,05 m	10,7
14	227 and 229	6816415,29577	440829,334402	7,15 m	25
Average				4,4 m	15,3 %

The intersections in table 4 are numbered after their location on the glacier, starting with intersection 1 near the glacier front. As can be seen from the table, the difference in depth is generally fairly small, with values ranging between 1 and 10 meters, except for intersection 3, 8 and 9. Intersection 9 is the one that really stands out, with a difference in ice thickness of almost 30 meters (section 5.2). Apart from intersection 9, the small depth difference (most values <5 m) between intersecting profiles supports the accuracy of the data interpretation and the GPS positions.

During fieldwork in March 2014, a snow layer of variable depth covered the glacier surface. The layer was thinnest along the centreline, with open patches of clear ice observed at irregular intervals. When moving the GPR over the surface of the snow layer, the glacier surface below will have a curved form on the profiles due to the higher amounts of snow along the glacial margins compared to at the centreline. The boundary between the snow and the underlying ice is clearly visible in one east-west profile (figure 21).

The velocity of electromagnetic waves in snow varies depending on density and water content, but is generally within $1.9\text{-}2.5 \cdot 10^8 \text{ ms}^{-1}$ (table 2). On March 25th, the snow was relatively dry and loose because of a long period of cold weather with moderate amounts of precipitation. The condition of the snow near the bottom of the layer is unknown, but it is likely much denser

than the surface snow due to the weight of the overlying snow packing the crystals together. A mid-range velocity of $2.2 \times 10^8 \text{ ms}^{-1}$ was assigned for finding the snow depth by using the measured two way time. Using this velocity as a basis for depth calculation in R2DQ, we found the thickness of the snow layer to be between 5 and 6 meters along the glacier margins, and approximately 1 meter along the centreline. This estimate is based upon a single profile, and snow depth is likely to both increase and decrease in relation to the topography further up the glacier. Since profile 159 was made at the end of the ablation season, there is no snow covering the glacier and the measurements were done directly on the glacier surface. With no snow layer, there is no curved reflector at the top of the profile (figure 22).

Another difference between profile 223 and 159 is the amount of hyperbolas (figure 21 & 22). In profile 159 there are several visible hyperbolas that do not follow the topography of the bottom reflector (figure 22), while no hyperbolas are visible in profile 223 (figure 21). Neither of these profiles have been processed with migration. As mentioned in (hyperbolas), hyperbolas occur when the GPR is moved over a buried discontinuity. There can be several reasons for why hyperbolas occur in profile 159 and not in profile 223. The amount of englacial rocks/boulders is likely not very different between the two profiles, and can be ruled out as a factor. When conducting the surveys in August/September, we were approaching the end of the ablation season and so the water content of the glacier is high. The speed of EM waves in water is much lower than in ice due to water having a higher relative permittivity (section [3.3.2](#)), meaning that pockets of water will act as point reflectors and therefore appear as hyperbolas on the radargrams (englacial films of water will be spread over a larger area and appear as a line). Equation 6 section [3.4.1.4](#) shows how reflection is based on EM wave speed through different media.

While surveying profile 159, the GPR had to be moved over several open crevasses while recording. The boundary between ice and air deeper in the crevasses can occur as a hyperbola on the radargrams due to the large difference in velocity between EM waves in air and in ice. When surveying in March 2014 most of the crevasses were partly filled with snow, creating a smoother transition between the crevasse and the glacier and thus avoiding large reflections.

Another factor to consider is the difference in resolution between the two antennas (section [3.4](#)), and the difference between the GPR parameters used. The 100 MHz antenna used to survey profile 159 gives a greater resolution and is capable of showing more details than the 50 MHz antenna. It is likely that there are reflectors in profile 223 that appear as hyperbolas in profile 159, but the lower frequency antenna used in profile 223 does not register them. In addition, as can be seen in figure 21 and figure 22, the two profiles were surveyed with different time interval settings (different horizontal resolution). Profile 159 has 375 traces, while profile 223 has only 80 traces along the same distance. Fewer traces means lower

horizontal resolution, and some reflectors could be hidden in profile 223 due to this. The difference between the two profiles is likely due to a combination of all 3 of these factors.

4.3 Ice thickness interpolation

4.3.1 2D-interpolation

Field measurements were not conducted on the whole glacier (figure 3). To estimate a volume for the whole glacier we had to interpolate data for the missing areas through the use of the interpolation lines shown in figure 21:

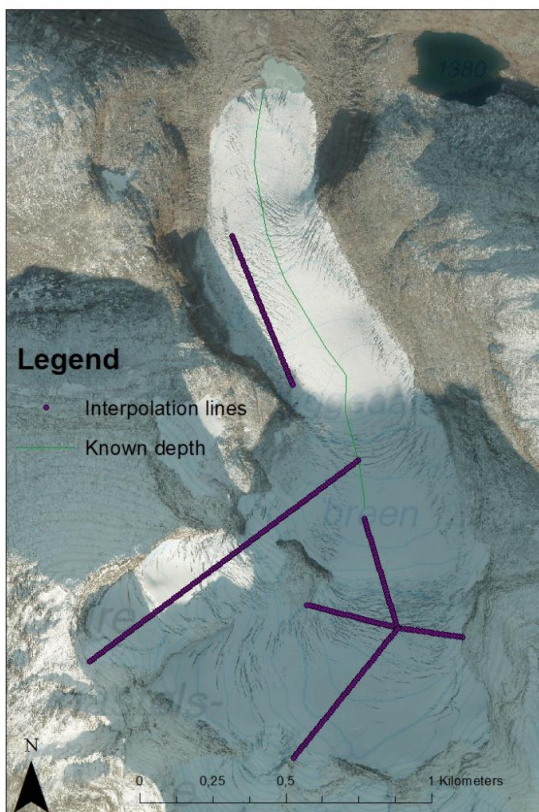


Figure 24: Figure showing interpolation lines and a reference line where the depth is known (green). The interpolation lines are calculated from known depth at a start and end point.

The interpolation lines had to be calculated from a function set in excel when depth at a start and end point was known. Along the green line shown in figure 24, several points had a known depth. From these we could calculate interpolation lines from the end of the green line towards points along the southern end of the glacier. The values of the interpolation line were shown as a graph in excel, and a function matching the interpolation was generated. An interpolation line

calculated from a second degree polynomial function is shown in figure 25 (linear function interpolation lines are shown in appendix 2):

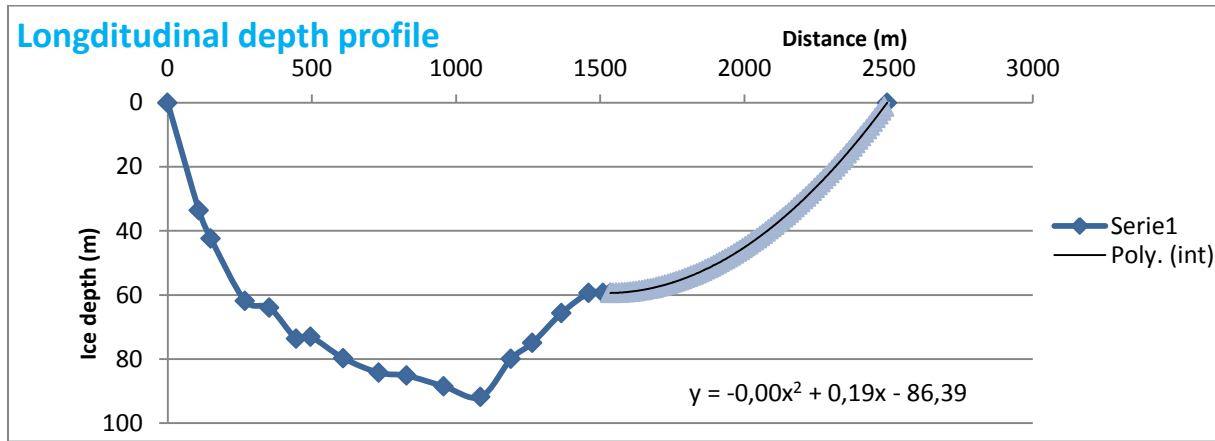


Figure 25: A longitudinal depth profile. The thick line is the interpolation line made from a function y .

4.3.2 3D-interpolation

To estimate a volume we need a 3-D interpolation for the whole glacier. To do this we need to mark the glacier boundary and assign a depth value of 0. Using the boundary, the depth values from the measured profiles and the interpolation lines, we can make an interpolation of the whole glacier. Figure 26 shows the profiles from which the depth calculation was done.



Figure 26: Boundary, interpolation profiles and profiles surveyed in the field (A). Glacier boundary, with depth equal to 0 (B).

The estimated glacier volume was calculated using the mapping and spatial analyst program in ArcGIS. Data from GPR profiles were imported and interpolation lines were made in order to have depth information for as large an area as possible. After merging the GPR profiles, interpolations and glacier boundary (figure 26), the whole glacier can be interpolated.

Several tools were used to acquire a good 3D-model. The geostatistical tool enabled us to use a radial basis function to make interpolations between points of known depth. With this tool a sector with four sections, with a 45 degree tilt, was used to optimize the distribution of GPR profiles. Since the glacier changes direction at the middle of the valley, two different interpolation models was made. This was because an average result for both directions combined would give a wrong depth model. The 5×5 grid cells in the two models were transformed into points containing depth information. The gap between the two models was interpolated and the models were merged together (figure 27).

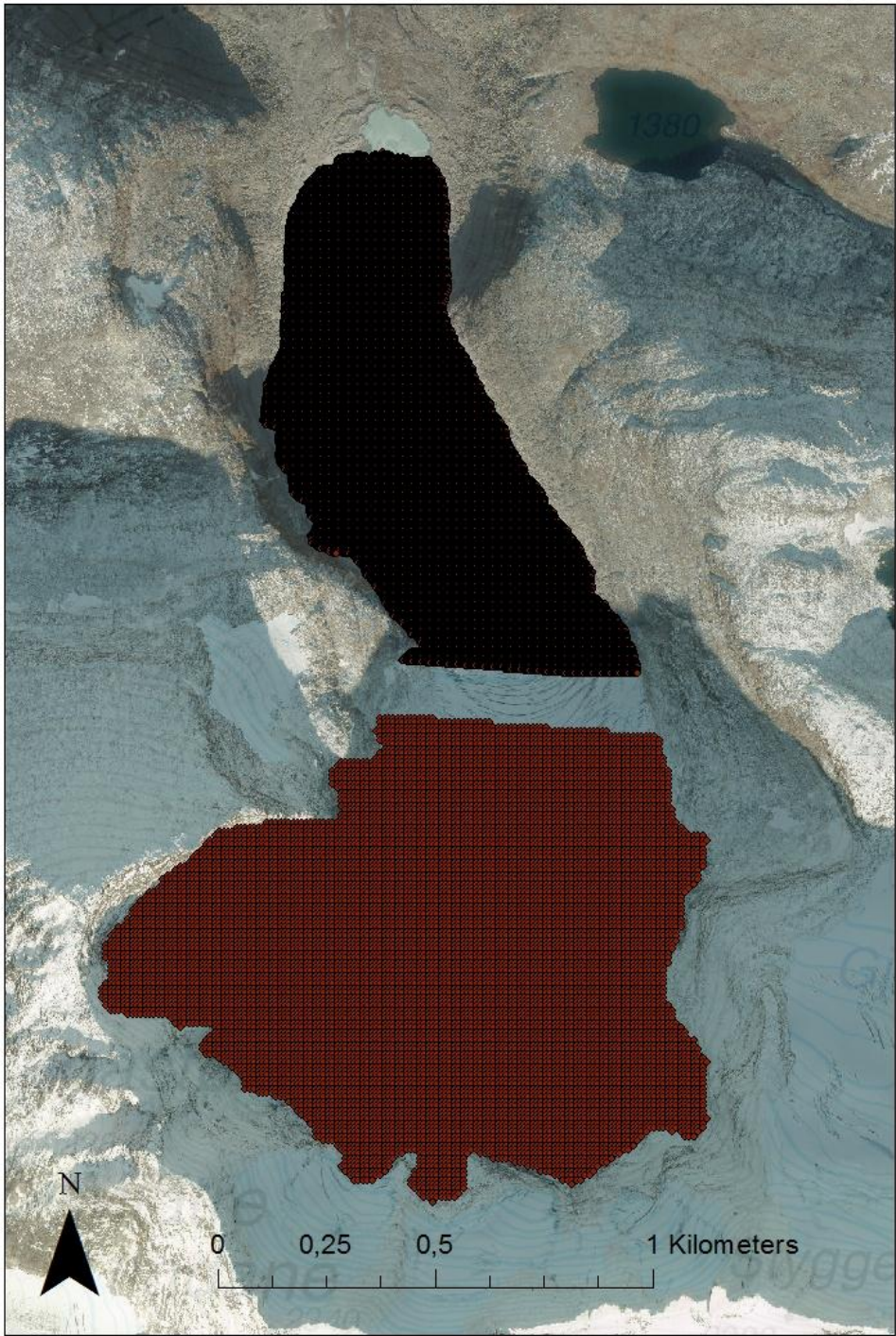


Figure 27: Merged layers containing grid codes with depth information. Two areas were merged: top of the glacier towards the south and the northern part towards the end of the glacier.

A depth model clipped to the glacier boundary was made (figure 25). Although similar to the final model, GPR profiles were still visible.

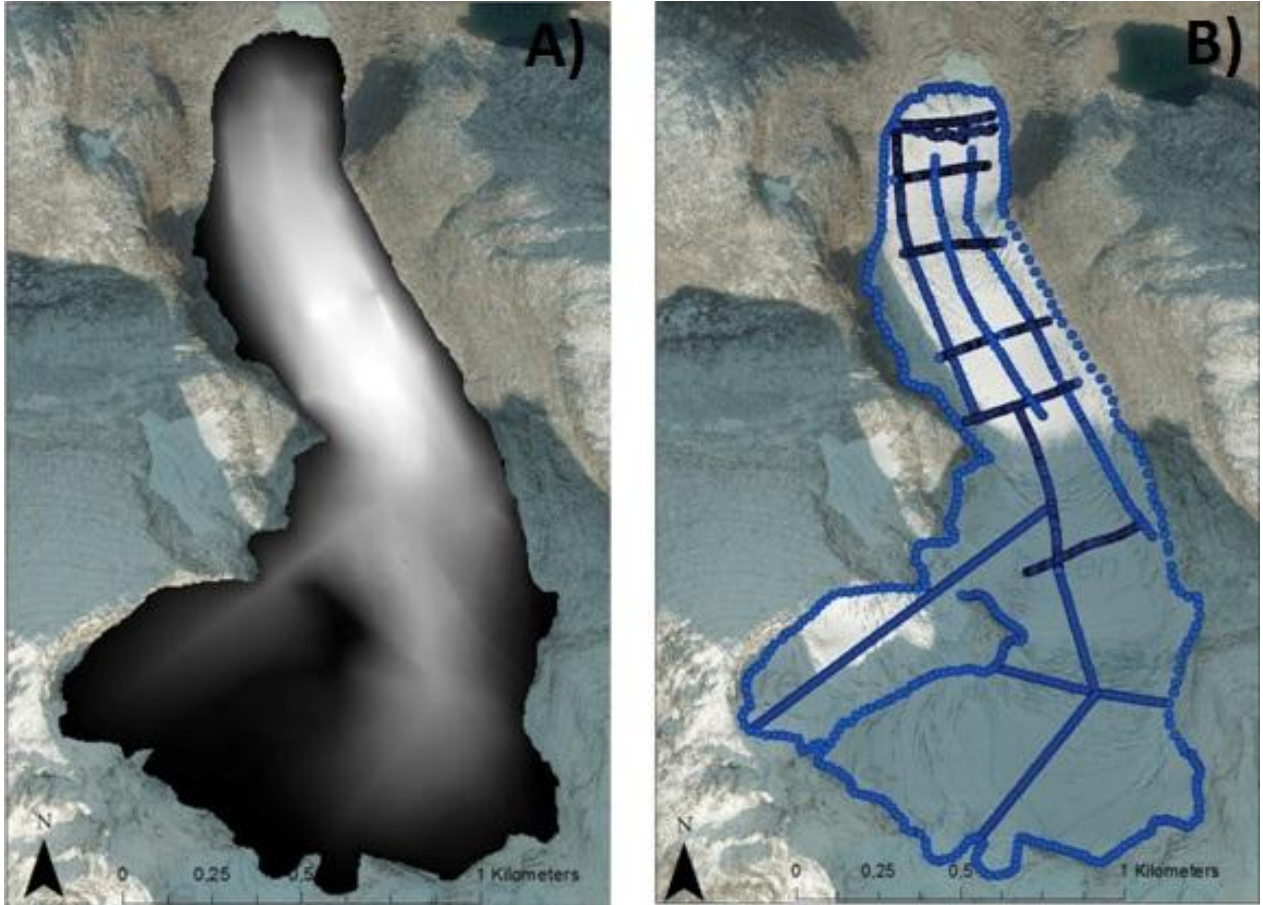


Figure25: Figure A is a depth model made from all known depths and the interpolation between them. Figure B shows all points for depth information. The profiles in figure B are visible in figure C as it has not been smoothed.

As a consequence we tested several smoothing routines and found that the ice thickness variation across Styggedalsbreen was best illustrated by increasing the cell size of the model. By increasing the cell size to 20×20 meters instead of 5×5 meters, no evidence exists of the GPR profiles in the ice thickness model (see figure 32).

4.4 Subglacial topography and variations in ice thickness

By subtracting the depth values given by the final ice thickness model from the DEM, we can make a model showing the subglacial bed topography using spatial analysis in ArcGis. The Subglacial topography model (Figure 29) presents a typical U-shaped valley with steep valley sides and a relatively flat bottom, which is typical for glacier eroded areas (Snl: Dal, 2007). The

bed topography is flat at the glacier tongue, but more undulating at the centre and steeper towards the eastern- and western margins (figure 27C). The steepening along the margins seems to happen all over the glacier, but it is less severe where the subglacial bed topography is flat and the supraglacial topography has a low inclination (figure 27A). At the centre of the glacier (south of point 1 in figure 26B) there is a steep slope leading up to a flatter area where the valley gets wider. This slope is even steeper at the subglacial bed, and the ice is thinner over the crest (figure 27). This explains the amount and size of the transverse crevasses we observed during our August-September surveys (section 2.3). At the southern end of the valley there is a large area surrounded by a steep rock wall to the south. Data for this area has been generated through interpolation, but the subglacial topography in the area appears realistic. The area with the greatest ice thickness is marked at point 1 in figure 26B. In this area the glacier rests on a bed with a low gradient, while in the southern part of the glacier the bed is steeper.

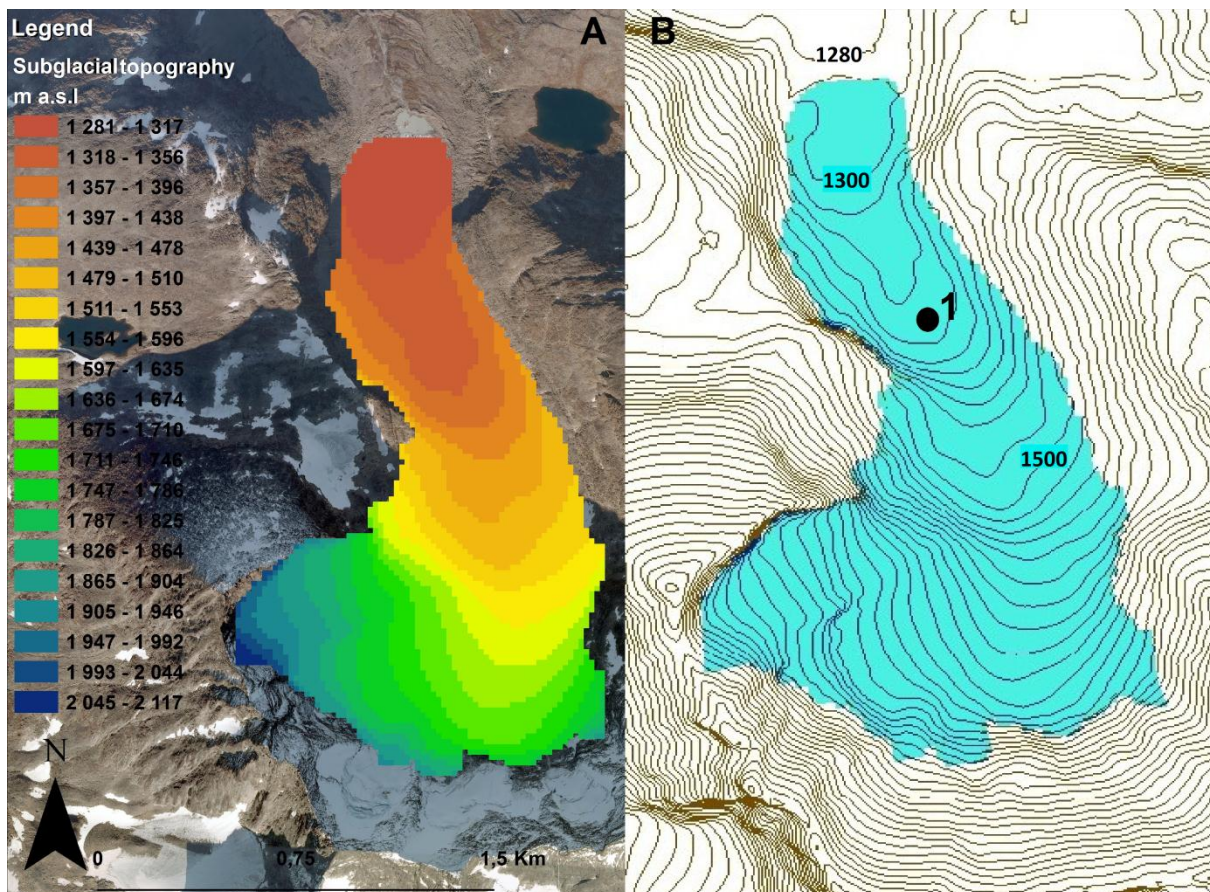


Figure 26: (A) Subglacial topography (m a.s.l.). (B) Point 1 shows area of highest observed ice thickness (98.7m)

The variation in ice thickness at Styggedalsbreen can be described in more detail by comparing the subglacial bed topography and the ice thickness model (Figure 27). The bed topography fluctuates and its influence on the supraglacial topography can be seen in figure 27C. The ice is thinner where

the subglacial bed is steep (figure 27B). This suggests that the build-up of ice is restricted in regions of steep subglacial topography.

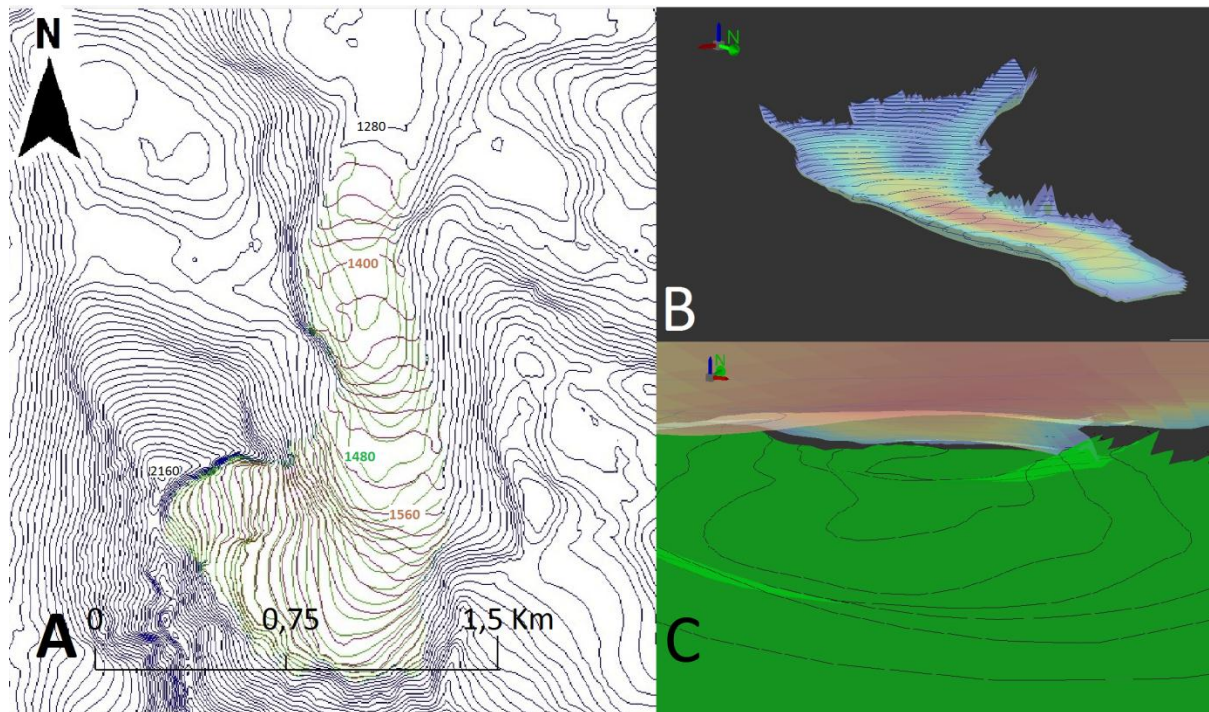


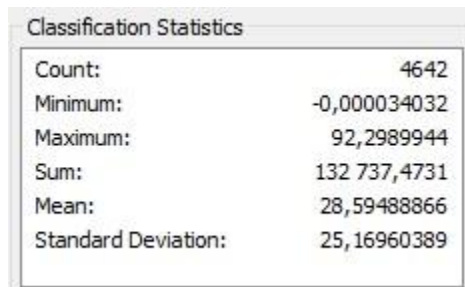
Figure 27: (A) Contour lines(20m) for subglacial (green) and supraglacial (red) topography. B gives a better impression of the ice thickness in different parts of the glacier. Contour lines illustrate variations in subglacial topography. Variations in supraglacial topography (colors ranging from red(high) to blue(shallow), showing ice thickness) and subglacial topography(green) from an englacial view looking north(from point 1; figure 26.)

4.5 Volume estimate

All of the processes mentioned above contribute to the main goal of this thesis, estimating the volume of Styggedalsbreen. From the ice thickness model presented below, we can calculate an estimated volume by multiplying the calculated mean depth with the number of 20*20m cells.

$$((20 \text{ m} * 20 \text{ m}) * \text{mean depth}) * \text{number of cells} = \text{estimated volume}$$

Inserting the numbers from figure 28 into this simple formula gives an estimated volume of Styggedalsbreen of $5.31 * 10^7 \text{ m}^3$, or 0.053 km^3 .



Classification Statistics	
Count:	4642
Minimum:	-0,000034032
Maximum:	92,2989944
Sum:	132 737,4731
Mean:	28,59488866
Standard Deviation:	25,16960389

Figure 28: Table showing values for the depth model. Cell count, minimum depth, maximum depth, sum of depth in all cells, mean depth and standard deviation from the mean depth. Minimum depth is negative because the interpolation at some points stretches beyond the boundary of the glacier, but it is such a small number that we ignore it and set it to 0.

Final ice thickness model is shown in figure 29

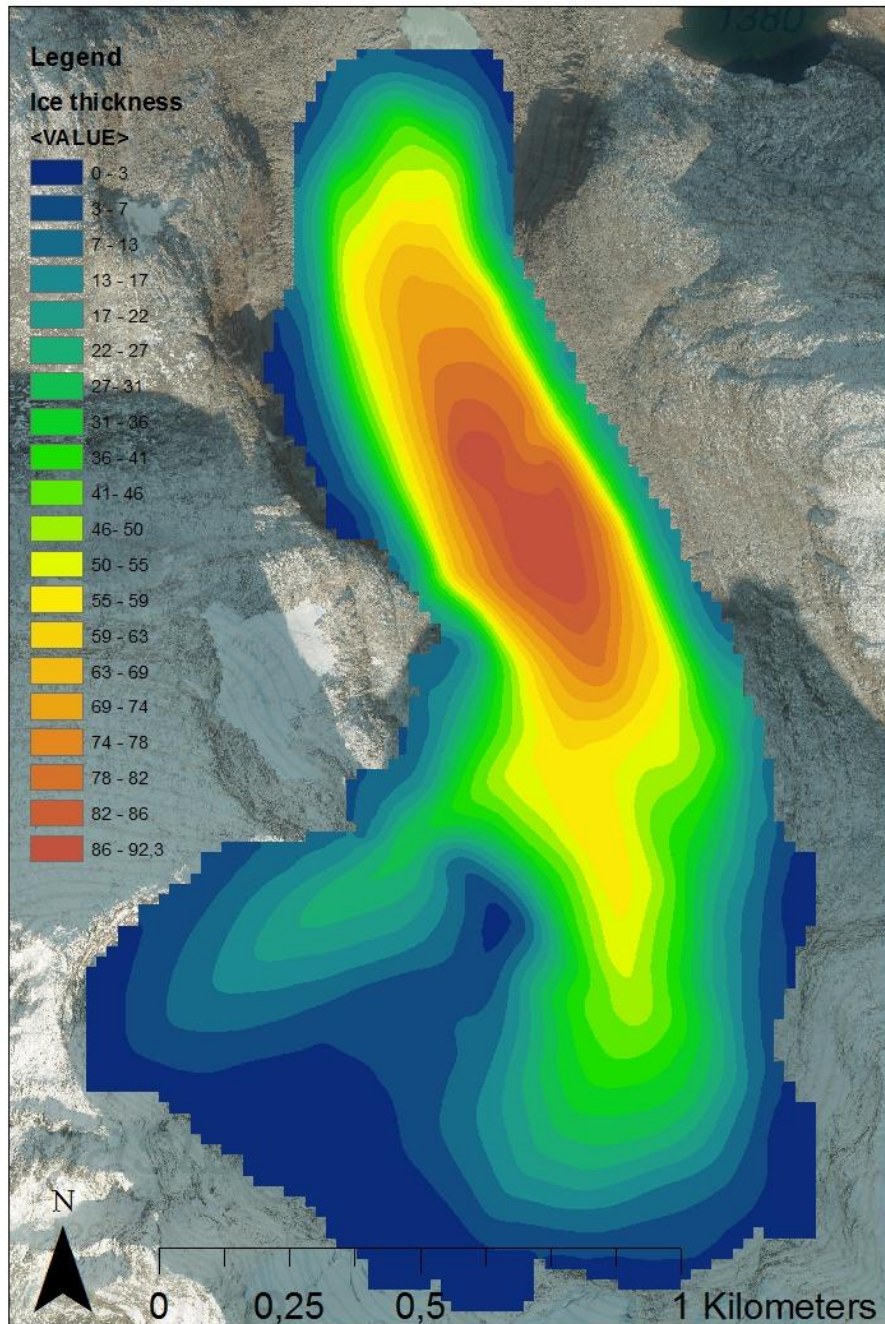


Figure 29: Ice thickness model of Styggedalsbreen glacier. Values are in meters.

Because of difference in density between water and ice, $5.31 \cdot 10^7 \text{ m}^3$ of ice equals $4.87 \cdot 10^7 \text{ m}^3$ of water (density of ice is approximately 0.917 kg/dm^3 , Sni: is-vann I fast form, 2007). The total weight of ice at Styggedalsbreen is $\sim 4.87 \cdot 10^{10} \text{ kg}$, or $4.87 \cdot 10^7$ tonnes.

4.5.1 LIA volume estimate

As mentioned earlier, NVE have been recording length change measurements at Styggedalsbreen since 1901, and have also made an estimate of the LIA surface area (NVE: Length change measurements of Styggedalsbreen). We can use this model to calculate an estimated volume of the 1750 version of Styggedalsbreen, and compare this to the glacier today. The surface area of Styggedalsbreen in 1750 is estimated to 3.11 km^2 , based on the location of the LIA moraine (NVE: Length change measurements of Styggedalsbreen). By combining the LIA surface area with the mean depth from this thesis, we can calculate an estimated volume. The mean depth of the glacier in 1750 was probably higher than it is today, and our calculations therefore represent a minimum value. However, modelling of the LIA surface is beyond the scope of this thesis and a rough estimate of the mean LIA ice thickness would be highly speculative, but is presented in the end of section [4.5.2](#). The surface area of Styggedalsbreen today is approximately 1.85 km^2 . This means the surface area of the glacier has been reduced by 1.26 km^2 since 1750. If the mean depth of 28.6 m is used, the volume of Styggedalsbreen at the LIA maximum was $\sim 0.089 \text{ km}^3$. The difference in volume is 0.036 km^3 , a decrease in volume of 40.5% over the last 250 years. It is important to keep in mind that this is a minimum value estimate, but it gives an impression of the difference in ice volume and rate of ablation since the LIA.

4.5.2 Volume-area empirical estimate

We can also compare our results against the general volume-area relation formula (Bahr *et al* 1997):

$$V = cA^\gamma \text{ equation 9}$$

Where the surface area is represented by A , while γ is a dimensionless scaling exponent with an approximate value of 1.375 for valley glaciers (Bahr *et al.* 1997). The formula uses the scaling coefficient c to account for whether the glacier, is in steady state or not. A glacier in steady state will have a c value of 1, while the c value for glaciers which are not in steady state will have to be calculated from surveys of the surface area and volume of the glacier.

If we use γ and c values suited for valley glaciers ($\gamma=1.36$ and $c=0.33 \text{ km}^{3-2\gamma}$, Bahr, 2011), and the area of Styggedalsbreen $A = 1.85 \text{ km}^2$ in equation 9, we get an estimated volume of 0.077 km^3 . If we do the same with the area from LIA, which is estimated to 3.11 km^2 (NVE: Length change measurements of Styggedalsbreen), it gives us an estimated volume of 0.157 km^3 . This is three times the volume today, and equals a LIA mean ice thickness of 50.4m. The volume estimate presented using today's mean ice thickness is approximately 76.4% smaller than 0.157 km^3 .

5 Discussion

5.1 Data collection

When using GPR to measure ice thickness, there are several uncertainties to consider. The conditions on the glacier decide the setup of the GPR parameters, and conditions are rarely uniform through the glacier interior. This is a problem that one will encounter no matter what, and the best solution is often to use settings that will give acceptable results through a range of different conditions.

Looking at the difference in ice thickness between profile intersections in table 4, section 4.2, the difference varies mostly between 1-10 m, with a mean difference of 6.2 m. If we exclude intersection 9, the mean difference is 4.4 m. Knudsen & Hasholt (1999) use a margin of error (m.o.e) of ± 5 m when discussing the uncertainty of GPR measurements. Because of the high water content of the glacier and the relatively high frequency of the 50 MHz antenna, uncertainties are likely to increase with depth (Yde, 2014). The EM velocity used in the March 2014 survey was set at $1.65 \cdot 10^8$ m/s (section 3.5), a velocity best suited for temperate ice. As is noted in the results section, the glacier surface is covered by a snow layer ranging in thickness from 5-6 m along the margins and 0-1 m along the centreline. With velocity set at $1.65 \cdot 10^8$ m/s, an additional error of 5-6 m is expected along the glacier margins. Overall, a m.o.e of approximately ± 8 m is likely.

We used different settings for the GPR time interval in the August/September surveys and the March survey. With a time interval of 0.5 s, the profiles from fall 2013 have a much higher horizontal resolution than the March profiles with a time interval of 2 s. Even though the profiles from March are generally better, a lower time interval would have increased the resolution and enabled us to see the profiles in greater detail. With a time interval of 2 s there might be reflectors that the GPR failed to register.

When doing the survey in March 2014, the snow cover enabled us to avoid crevasses and rock fall debris and to measure the profiles in a relatively straight line. Maintaining correct antenna separation was a challenge during the August/September surveys, because the antennas would get stuck behind large rocks and boulders or slide off track on the clear ice. Wrong antenna separation can cause the GPR to misregister reflectors, or even to not register them at all. This can cause an abnormal level of noise and/or artefacts on the radargrams, making interpretation more difficult.

The profiles are placed in a grid pattern across the glacier in order to give a relatively detailed view of the bottom topography (figure 20). Due to time restraints, concerns for the longevity of the batteries and large amount of rock fall debris, we did not measure all the way across the glacier on the east-west profiles, but skipped the last 10 meters towards the valley side on both sides. These 10 meters are not that important, as we know the glacier depth will gradually decrease towards 0 as we approach the margins. The snow cover also made it difficult to know whether we were walking on the glacier or had crossed the glacier margin. An increased number and density of profiles on the glacier would have increased the accuracy of the volume estimate. Profiles across the whole glacier would have been preferable, but as noted earlier, the southernmost area was deemed too dangerous to enter, and depth data for this area had to be interpolated from the other profiles.

All profiles from 2013 were recorded with the Globalsat BU-353 usb gps in addition to a backup handheld GPS. The m.o.e when using GPS is between 5-10 m horizontally and 1.5 times that vertically, depending on the topography and landscape at the location. Tight valleys and high alpine peaks can disrupt the signal, and thereby degrade the accuracy of the GPS further (Trimble navigation Limited, 2011) When the Globalsat USB GPS and the backup handheld GPS failed during the March 2014 survey, the Suunto GPS watch functioning as a 2nd backup was the only source of GPS data available. The watch itself is no less accurate than a normal GPS, but the unconventional method we used to extract the GPS data (section [3.7](#)) increases the m.o.e by an unknown amount. However, looking at the depth difference at profile intersections, the relatively small difference in depth suggests that the profiles are located correctly and that the method has provided reliable results (table 4: section [4.2](#)).

5.2 Interpretation and interpolation

RadExplorer and R2DQ GPR interpretation software were used to interpret the radargrams. While providing the same base functions, the quality of the processed profiles sometimes varied significantly. RadExplorer is supported by Malå, the manufacturer of the GPR, and should in theory be better suited for the interpretation of the radargrams than R2DQ. While having a more user friendly interface, the poor customizability and GPS data processing functions of RadExplorer meant that we sometimes used RadExplorer for interpretation and R2DQ for calculating GPS coordinates. If RadExplorer was used for interpreting the profiles, we always transferred the interpretation into R2DQ to be able to correctly merge the radargrams with the GPS data and to avoid getting conflicting results due to software differences.

Few profiles gave a clear image of the ice-bed interface from the start, and most had to go through processing and comparison with neighbouring profiles to be able to provide a satisfactory interpretation of the subglacial topography. Several of the profiles from the 1st and 2nd survey in 2013 were very difficult to interpret, with hyperbolas and other artefacts and structures appearing seemingly at random (section 4.2). The large uncertainties concerning the results of these surveys were part of the reason we did another survey during the accumulation season in March 2014. The profiles from 2014 were collected with a 50 MHz antenna instead of 100 MHz as in September 2013, effectively reducing the resolution but increasing the penetration depth (section 3.4). The higher quality of the March 2014 radargrams are likely due to lower water content, fewer open crevasses and different antenna and GPR settings.

There are several uncertainties related to the processing of the profiles, including locating the correct reflector and using filters to amplify the desired signal frequency while removing unwanted noise. The uncertainties increase with depth because of the limitations of the 100 MHz and 50 MHz antenna. Generally, the deeper the profile the more difficult it gets to locate and enhance the bottom reflector. Choosing the wrong reflector will have an impact on the final volume estimate.

Side-swipes (section 3.4.3) can cause problems along longitudinal profiles. An effective way to deal with side-swipes is to use migration during processing, but migration was not used on every profile (Appendix a) because it caused a loss of signal strength. This could lead to misinterpretation of the reflectors.

Another source of error is the aerial photos used to calculate the surface area of Styggedalsbreen. Bygdin 2008 and Sogn 2010 were imported into ArcGis and used as a basis for area calculations together with the Toporaster2 WMS (www.norgebilder.no). From 2008 to 2010 the glacier retreated 27 m, and from 2010 to 2013 it retreated another 33 m (NVE Length change measurements of Styggedalsbreen). This change in length affects the total surface area, and is not taken into account when performing the volume calculations. The area calculations based on Bygdin 2008 show a surface area of approximately 1.85 km², a slight overestimation considering the glacier retreated 60 m from 2008 to 2013. A retreat of 60 m equals a loss of surface area of approximately ~15000 m², or ~0.8% since 2008. This means that since the calculations are based on the surface area from 2008, the final volume estimation is an overestimation of the real volume by ~0.8 %. NVE uses a surface area estimate of 2 km² for Styggedalsbreen, but this number is from 2003 when the glacier extended almost 100 m further north than today (NVE: Length change measurements of Styggedalsbreen).

In order to guide the 3D-interpolation, the depth and shape of the bottom topography found in the southernmost GPR profiles was used to interpolate ice thickness into the southern area of Styggedalsbreen where no measurements exist. This is of course less than optimal for volume

estimation, but with no real data from this area, an interpolation along chosen profiles provides a good alternative. Another option was to draw a straight line from the southern profiles towards the southern end of the glacier and have the depth gradually decrease towards 0 along this line. This is the method we used to interpolate the south-western arm of the glacier. Both methods create uncertainties when used in combination with volume estimations, but the interpolation based on existing profiles creates a somewhat more realistic result. Uncertainties concerning interpolated values will increase with distance from a known measurement.

The large difference in ice thickness observed at intersection 9, table 4, could be due to a number of reasons. This intersection is located close to the glacier margin where the snow layer is thickest and there is an abundance of chevron crevasses (figure 3). The combination of a thick snow layer and crevasses that possibly contain water or debris can cause misinterpretation of the profiles, thus leading to the difference in observed thickness. Another possibility is the subglacial valley side causing side swipes, but the longitudinal profile (229) has been migrated while the cross profile (233) has been processed both with and without migration (Appendix a). This decreases the likelihood of side swipes causing the difference in ice thickness.

5.3 Volume estimations

The volume estimate is calculated using a fairly simple formula based on mean depth and total surface area divided into cells (section [4.5.2](#)). By using a model resolution of 20 m x 20 m, the volume model maintains a fair level of detail, while, at the same time, recognizing that the ice thickness in many regions relies largely on interpolated values. The 400 m² squares creates a “blocky” looking model with some squares crossing the glacier boundary. The area outside the glacier boundary covered by the model is offset by an approximately equal area of the glacier that is not covered, and the error associated with this is therefore likely minor.

Using a margin of error of ± 8 m, the volume estimate of 0.053 km³ is a middle value between a minimum volume of ~ 0.039 km³ and a maximum volume of ~ 0.068 km³. This equals a margin of error of approximately 28 %, which is quite high. It is important to remember that this high percentage is due to the relatively low mean ice thickness. As an example, a mean thickness of 100 m ± 8 m would give a margin of error of 8%. A m.o.e. of ± 8 m is probable at the thicker parts of the glacier, but not very likely towards the glacier margins where the thickness approaches 0 m. Thus, to achieve a more realistic margin of error, we calculated the average difference using the variations in ice thickness found in table 4. This gave us a margin of error of approximately 15.3 %. Since the ice thickness in most of the intersections is greater than the mean value of 28.6 m, the calculations present a lower number than 28 %. Note that

intersection 9 is excluded from these calculations. If we add the m.o.e. from the aerial photos, the total m.o.e. is approximately 16.1 %. Based on a m.o.e. of 16.1 %, the minimum volume estimate of Styggedalsbreen is $\sim 0.044 \text{ km}^3$ and the maximum estimate is $\sim 0.062 \text{ km}^3$. This presents a more realistic minimum/maximum estimate than when using a m.o.e. of 28 %.

With no previous research on the volume of Styggedalsbreen, we have to rely completely on our own findings. This may in itself be both a strength and weakness of the thesis, as it forces us to look at the data with a critical eye and strive to achieve a high level of accuracy. At the same time, the lack of other sources of data means that we have little to compare our results and methods to. However, we can compare our results against the general volume-area relation formula (section [4.5.2](#)). With a difference of 0.024 km^3 , or 45.3 %, between the estimate of this thesis and the volume-area estimate found using equation 9, it is clear that the volume area formula, when seen in relation to this thesis, is not yet optimized for estimating a global glacier volume. It is possible that the formula overestimates the volume of Styggedalsbreen because uncertainties concerning ice thickness have a greater impact on the volume estimation of small glaciers, and that it would provide a better result when used on larger glaciers. More accurate values for c and γ could have improved the estimate as well. If the volume estimation calculated from equation 9 was a correct presentation of today's situation, the mean ice thickness of Styggedalsbreen would have been approximately 41.6 m.

The LIA volume estimate presented in section...is based on the mean ice thickness of Styggedalsbreen found in this thesis. As noted, the increased surface area during the LIA means that the mean thickness was likely higher than today, and the estimate presented is thus a minimum estimate. When the volume-area formula is applied to the LIA surface area, the calculated volume is twice as large as the minimum LIA volume estimate and 3 times as large as the volume of Styggedalsbreen today. This highlights some of the same problems noted above, that the volume-area formula seems to overestimate the actual volume, and that it is hard to calculate a correct estimate without accurate values for c and γ .

6 Conclusion

The maximum ice thickness is 98.7 ± 8 m and the mean thickness is 28.6 ± 8 m. This is based on the maximum m.o.e. of GPR measurements in combination with snow depth. The ice thickness was calculated from the interpolation between GPR profiles, interpolation lines and a 0-depth glacier boundary. The final estimated volume was calculated to be 0.0529 ± 0.0085 km³, or $5.29 \pm 0.085 \times 10^7$ m³. This is based on a m.o.e. of 16.1 %. Uncertainties are based on the profile intersections (table 4) and the mean snow depth.

Decrease in glacier volume since the LIA was calculated from the location of the LIA moraine in combination with the mean ice thickness of today. The LIA volume estimate of 0.089 km³ suggests that Styggedalsbreen has lost ~40.5 % of its volume over the last 250 years. 0.089 km³ is a minimum estimate, and so the glacier might have lost more than this.

The estimated volume cannot be compared to other sources of data since no other volume measurements have been done on Styggedalsbreen. However, we can calculate a volume from an empirical volume-area equation and give an estimate for what the volume should be according to this formula. An estimation using the volume-area formula suggests a volume of ~0.077 km³, an overestimation of 45.3 % compared to the volume estimated in this thesis. The results of this thesis can, when combined with volume research of other glaciers in a similar environment, help improve the volume-area formula and adapt it towards a wider range of glaciers. When predicting future GMSL, it is important to have as accurate data as possible concerning the contributions from melting glaciers and ice caps.

Based on experience and knowledge gained during the making of this thesis, a number of recommendations for future research can be given:

After surveying both at the end of the ablation season and at the end of the accumulation season, it is clear that the latter gave best results. During the March 2014 survey, the whole glacier was covered with snow. This provided good accessibility for most parts of the glacier; mainly due to the closing of crevasses and the smooth supraglacial surface. The water content is also lower than during the ablation season due to less melting, and that precipitation comes mainly in the form of snow.

The antenna frequency choice is also important in order to obtain the best results. Higher frequencies may give good resolution but often at the expense of the penetration depth. Although energy loss in ice is relatively low, the presence of water, crevasses, impurities (debris, rocks etc.) can cause unwanted reflectors in the glacier and thus leave crucial boundaries undetected. As mentioned, both a 100 MHz RTA and 50 MHz RTA were used in the GPR surveys. The 50 MHz RTA gave better results and was able to register reflections down to a

depth of 98.7 ± 8 m. In comparison, the maximum ice thickness observed with the 100 MHz antenna was 50.8 m (based on profile 159, figure 20). For further investigations, a lower frequency antenna, for example 30 MHz or lower, is recommended. This will lead to a higher penetration depth and a better chance of registering deep boundaries.

The distribution of profiles within the survey grid should be considered carefully when planning a survey. The higher the density of the profiles, the less impact it has if reflectors appear to be inconclusive. Hence the interpretation and depth calculations will prove to be more conclusive and accurate.

A GPS is important in order to connect the traces and the interpreted ice thickness to the correct positions on the glacier. Out of experience, it is very important to bring a second and third back-up GPS device.

Aerial photos used in ArcGIS or other mapping or spatial analysis programs have been taken at certain times. It is important to account for the ablation or accumulation of the glacier in the time between the GPR survey and the capturing of the photo. Have in mind that areal data is not always available, although NVE carries out length and area surveys on several glaciers.

Acknowledgements

We wish to thank associate professor Mette Kusk Gillespie for invaluable guidance and corrections of this bachelor thesis, and associate professor Simon de Villiers for supplying us with articles and literature, and for answering questions on the fly. Big thanks also go to associate professor Jacob C. Yde for great lectures and general answers about glaciology. Furthermore, we want to thank Luster Red Cross for helping us with transportation from Turtagrø to Styggedalsbreen during our survey in March 2014, and Turtagrø Hotel which let us charge batteries and use their bathroom facilities.

Last, but not least, we want to show our appreciation of the study facilities and study environment at Høgskulen i Sogn & Fjordane, to which all our fellow students and lecturers contribute.

References

- Andreassen, L.M., Hausberg, J.E., Paul, F. & Winswold, S.H. (2012) *Inventory of Norwegian Glaciers*. Oslo: Norwegian Water Resources and Energy Directorate (38-2012)
- Askheim, S. & Thorsnæs, G. (2014) *Jotunheimen*. Available at: <http://snl.no/Jotunheimen#menuitem2> (Accessed: 29.01.2014).
- Bahr, D.B., Meier, M.F. and Peckham, S.D. (1997). *The physical basis of glacier volume-area scaling*. *Journal of Geophysical Research* volume 102, p. 20,356. Available at: <http://onlinelibrary.wiley.com/doi/10.1029/97JB01696/full> (Accessed 20.05.20014).
- Bahr, D.B. (2011). Estimation of glacier volume and volume change by scaling methods. In Singh, V.P., Singh, P., Haritashya, U.K. (editors): *Encyclopedia of snow, ice and glaciers*, Springer, Dordrecht, The Netherlands, p. 278-280.
- Bahr, D.B., Dyurgerov, M., Meier, M.F. (2009): Sea-level rise from glaciers and ice caps: A lower bound. *Geophysical Research Letters*, 36, L03501, doi: 10.1029/2008GL036309.
- Barry, R.G. (2005) *Mountain Weather & Climate*. 2nd edition. London: Routledge, p. 126-137.
- Benn, D.I. & Evans, D.J.A. (2010) *Glaciers & Glaciation*. 2nd edition. London: Hodder Education, p. 36, 134-137.
- Bedrock geology-N250 Raster map* (2014) Available at: <http://geo.ngu.no/kart/arealisNGU/> (Accessed: 12.05.2014).
- Bex and P.M. Midgley (eds.)).Cambridge University Press, Cambridge, United Kingdom and New York, NY, USA. p. 90. Available at <http://ipcc.ch/report/ar5/wg1/>. (Accessed: 25.05.2014).
- Birkenfeld, S. (2010) "Automatic detection of reflexion hyperbolas in GPR data with neutral networks". World Automation Congress. P. 5
- Bradford, J.H and Harper, J.T. (2005) *Wave Field Migration as a Tool for Estimating Spatially Continuous Radar Velocity and Water Content in Glacier*. Center for Geophysical, Investigation of the Shallow Subsurface (CGISS). P. 3-5.
- Brandt, O. (2007) *Application of Ground penetrating Radar as a tool for Cryosphere Characterization*. Ph.D. Thesis. University of Oslo. P. 11-22.

Bryhni, I. (2011) *Jotundekket*. Available at: <http://snl.no/Jotundekket> (Accessed: 12.05.2014).

Church, J.A., P.U. Clark, A. Cazenave, J.M. Gregory, S. Jevrejeva, A. Levermann, M.A. Merrifield, G.A. Milne, R.S. Nerem, P.D. Nunn, A.J. Payne, W.T. Pfeffer, D. Stammer and A.S. Unnikrishnan, 2013: Sea Level Change. In: *Climate Change 2013: The Physical Science Basis. Contribution of Working Group I to the Fifth Assessment Report of the Intergovernmental Panel on Climate Change* [Stocker, T.F., D. Qin, G.-K. Plattner, M. Tignor, S.K. Allen, J. Boschung, A. Nauels, Y. Xia, V. Bex and P.M. Midgley (eds.)]. Cambridge University Press, Cambridge, United Kingdom and New York, NY, USA. Chapter 13, (PDF). p.1151, 1180. Available at <http://ipcc.ch/report/ar5/wg1/>

Daniels, J.J. (2000) *Ground Penetrating Radar Fundamentals*. Department of Geological Sciences, The Ohio State University. P. 4-5.

eKlima. (2014) Meteorologisk institutt. Available at: http://sharki.oslo.dnmi.no/portal/page?_pageid=73,39035,73_39049&_dad=portal&_schema=PORTAL (Accessed 28.04.2014).

Førre, E. (2012) *Topografi og dreneringsretninger under Nordfonna*. MSc. University of Bergen, Department of Earth Sciences.

Fylkeatlasing (2014) Available at: <http://www.fylkesatlas.no/default.aspx?gui=1&lang=3> (Accessed 29.01.2014).

Gidusko, K. *GPR Testing At St. Augustine's Fountain Of Youth Archaeological Park*. Available at: <http://fpangoingpublic.blogspot.no/2014/01/gpr-testing-at-st-augustines-fountain.html> (Accessed: 09.06.2014).

Hubbard, B and Glasser, N (2005). *Field techniques in glaciology and glacial geomorphology*. Centre for Glaciology, University of Wales, Aberystwyth. P. 148-155, 171-174.

IPCC 2001. *IPCC Third Assessment report: Climate Change 2001*. Chapter 11.2.3. Available at: http://www.grida.no/publications/other/ipcc_tar/?src=/climate/ipcc_tar/wg1/416.htm (Accessed: 01.06.2014).

Kartverket (2014). *Digital elevation model 10 m, UTM 33, Luster*. Available at: <http://data.kartverket.no/download/content/digital-terrengmodell-10-m-utm-33> (Accessed: 05.05.2014)

Knudsen, N.T. & Hasholdt, B. (1999) *Radio-echosounding at the Mittivakkat Gletscher, Southeast Greenland*. Arctic, Antarctic and Alpine Research, p. 324.

MALÅ Geoscience. (2011a) ProEX - Professional Explorer Control Unit. Operating Manual v. 2.0. 19-001030.

Mussett, A.E. and Khan, A.M. (2000) *Looking Into the Earth*. New York: Cambridge University Press. P. 227-231, 210-211, 217-220.

Nesje, A., Bakke, J., Dahl, S.O., Lie, Ø. and Matthews, J.A. (2008) "Norwegian mountain glaciers in the past, present and future". *Global and Planetary Change*, 60 (PDF) .p. 15.

Norgeskart (2014) Available at: <http://www.norgeskart.no/#5/378604/7226208> (Accessed 29.01.2014)

Norges vassdrags- og energidirektorat (NVE). *Length change measurements of Styggedalsbreen*. Available at: <http://glacier.nve.no/viewer/ci/en/nve/ClimateIndicatorInfo/2680> (Accessed: 15.04.2014).

Plewes, L.A and Hubbard, B. *A review of the use of radio-echo sounding in glaciology*. *Progress in Physical Geography* 2001 25: 203. P. 2-12

Salinger, j. et al. (2008) *glacier response to climate change*. Water and atmosphere (3). Available at: <https://www.niwa.co.nz/sites/niwa.co.nz/files/import/attachments/glacier.pdf> (Accessed: 08.06.2014). P. 16.

Sandmeier, K-J. *Reflex 2D-Quick guide*. Sandmeier geophysical software. Available at: <http://www.sandmeier-geo.de/Download/reflex2dquick.pdf> (Accessed: 10.06.2014). P. 13-14.

Stocker, T.F., D. Qin, G.-K. Plattner, L.V. Alexander, S.K. Allen, N.L. Bindoff, F.-M. Bréon, J.A. Church, U. Cubasch, S. Emori, P. Forster, P. Friedlingstein, N. Gillett, J.M. Gregory, D.L. Hartmann, E. Jansen, B. Kirtman, R. Knutti, K. Krishna Kumar, P. Lemke, J. Marotzke, V. Masson-Delmotte, G.A. Meehl, I.I. Mokhov, S. Piao, V. Ramaswamy, D. Randall, M. Rhein, M. Rojas, C. Sabine, D. Shindell, L.D. Talley, D.G. Vaughan and S.-P. Xie, 2013: *Technical Summary*. In: *Climate Change 2013: The Physical Science Basis Contribution of Working Group I to the Fifth Assessment Report of the Intergovernmental Panel on Climate Change* [Stocker, T.F., D. Qin, G.-K. Plattner, M. Tignor, S.K. Allen, J. Boschung, A. Nauels, Y. Xia, V.

Store norske leksikon: is - vann i fast form (2007) Available at: [http://snl.no/is%2Fvann i fast form](http://snl.no/is%2Fvann_i_fast_form) (Accessed: 01.06.2014).

Store norske leksikon: Dal (2007). Available at: <http://snl.no/dal> (Accessed: 09.06.2014).

Trimble Navigation Limited. (2011) Trimble Floodlight Technology. Available at: http://www.geoteam.dk/files/manager/mobil-gis-gps-til-dataindsamling/floodlight_technology_brief.pdf (Accessed: 25.06.2014). P. 1-2.

U.S. Department of Transportation. *Ground-Penetration Radar*. Available at: <http://www.cflhd.gov/resources/agm/engApplications/BridgeSystemSubstructure/243GroundPenetratingRadar.cfm> (Accessed: 02.06.2014).

Weatherbase. *Southpole, Antarctica*. Available at: <http://www.weatherbase.com/weather/weather.php3?s=90098&cityname=South-Pole-Antarctica&units=metric> (Accessed: 06.06.2014).

Yde, J.C., Riger-Kusk, M., Løland, R., Ruud, H., Mernild, S.H., Villiers, S.d., Knudsen, N.T., and Malmros, J.K. (2014). *Volume-area scaling at Mittivakkat Gletscher, Southeast Greenland*. Submitted to *Journal of Glaciology*.

Appendix A:

Processing tools (with values):

profiles	Static correction	Subtract-mean(dewow)	Gain function	Bandpass butterworth	Background removal	Migration	Plot scale
159	ON	ON: 30	Linear: 0,15. Exp.: 0,25	Low: 10 High: 50	ON	ON: 165	
223	ON	ON: 30	Linear: 0,1 Exp.: 0,2	Low: 12,5 High: 60	ON	ON: 0,1194 165	
162	ON	ON: 30	Linear: 0,2 Exp.: 0,35	Low: 12,5 High: 70	ON	ON: 0,073 165	
224	ON	ON: 30	Linear: 0,15 Exp.: 0,25	Low: 12,5 High: 50	ON	ON: 0,075 165	
226	ON	ON: 30	Linear: 0,15 Exp.: 0,3	Low: 12,5 High: 60	ON	ON: 0,046 165	
227	ON	ON: 30	Linear: 0,1 Exp.: 0,25	Low: 12,5 High: 50	ON	ON: 0,080 165	
229	ON	ON: 30	Linear: 0,15 Exp.: 0,25	Low: 12,5 High: 60	ON	ON: 0,028 165	
230	ON	ON: 30	Linear: 0,05 Exp.: 0,15	Low: 12,5 High: 60	ON	ON: 0,2377 165	
232	ON	ON: 30	Linear: 0,15 Exp.: 0,2	Low: 12,5 High: 80	ON	Off/ ON: 165	0,061
233	ON	ON: 30	Linear: 0,15 Exp.: 0,25	Low: 12,5 High: 70	ON	Off/ ON: 165	0,05
234	ON	ON: 30	Linear: 0,1 Exp.: 0,15	Low: 12,5 High: 60	ON	Off/ ON: 165	0,05
235	ON	ON: 30	Linear: 0,15 Exp.: 0,22	Low: 12,5 High: 60	ON	Off/ ON: 165	0,076

Values used for processing the GPR profiles.

List of abbreviations:

Abbreviation	Meaning	Page first mentioned
RTA	Rough terrain antenna	23
GPR	Ground Penetrating Radar	13
R2DQ	Reflex2D-Quick	34
GIS	Geographic Information System	Abstract
NVE	Norges Vassdrag og Energidirektorat	13
DEM	Digital Elevation Model	14
m a.s.l	Meter above sea level	15
GMSL	Global Mean Sea Level	11
ELA	Equilibrium Line Altitude	15
LIA	Little Ice Age	21
EC	Electric Conductivity (microsiemens per meter)	24
EM	Electro Magnetic	23
GPS	Global Positioning System	34
m.o.e	Margin of error	57

Appendix B:

Appendix attached to CD-R

Contents:

1. Shape files (ArcMap)
 - 1.1. Final depth model
 - 1.2. Interpolation lines
 - 1.3. GPR profiles
 - 1.4. General shapefiles
2. Interpolation lines (UTM calculations)
3. Reflex2DQuick
 - 3.1. Processed profiles (with interpretation)
 - 3.2. Unprocessed profiles